Available online at www.sciencedirect.com
ScienceDirect
Coordination Chemistry Reviews 251 (2007) 1796–1821
COORDINATION CHEMISTRY REVIEWS
www.elsevier.com/locate/ccr

Review

Density functional theory applied to calculating optical and spectroscopic properties of metal complexes: NMR and optical activity☆

Jochen Autschbach

Department of Chemistry, 312 NSC, State University of New York at Buffalo, Buffalo, NY 14260-3000, USA

Received 9 November 2006; accepted 12 February 2007
Available online 21 February 2007

Contents

Abstract

A short overview of the theoretical approach to calculate linear response properties (double perturbation properties) for molecules is given. The importance of response calculations to determine various spectroscopic parameters is outlined. The formalism covers static (time-independent) and dynamic (time-dependent) perturbations. Two areas of research where such theoretical methods are of practical importance are the computation of NMR parameters and computations of response functions that govern the optical activity of a molecule. An account of recent work by the author and collaborators based on density functional theory as applied to the computation of NMR chemical shifts and spin–spin coupling and to circular dichroism and optical rotation of metal complexes is presented. Among other topics, relativistic effects, solvent effects, and vibrational corrections are discussed.

Keywords: Transition metal complexes; Computational chemistry; NMR; Optical activity; Relativistic effects; Solvent effects; DFT computations

1. Introduction

The computation of properties of metal complexes by utilizing first-principles (ab initio) quantum theoretical methods has traditionally met with great challenges. Even as recent as 10–15 years ago, most first-principles computations on metal

☆ Based on a keynote lecture presented at the 37th International Conference on Coordination Chemistry, 13–18 August 2006, Cape Town, South Africa.

E-mail address: jochena@buffalo.edu.

0010-8545/$ – see front matter © 2007 Elsevier B.V. All rights reserved.
doi:10.1016/j.ccr.2007.02.012

complexes have not been able to match the expectations of experimental chemists in their ability to reproduce experimental data, to predict yet unavailable measurements with confidence, or to support assignments of spectra and analyses of optical and spectroscopic properties with the help of theoretical results that agree well with experiment. Instead, semi-empirical methods were in widespread use. It is fair to state that the situation has changed tremendously in the meantime; few chemists today question the value of ab initio theoretical support in their research.

It is widely recognized that both the advances in affordable computer hardware and many break-through method developments in quantum chemistry have contributed to the success-story of ab initio computational coordination chemistry. This article will focus on applications of some of the quantum chemical methods developed during recent years. It is now possible not only to explore the chemistry of metal complexes computationally – a task defined in the context of this paper as the computation of the energy of a metal system as a function of geometry, i.e. isomers, conformers, reactants, products, transitions states, and so on – but also to a satisfactory degree their optical and spectroscopic properties. Such properties can be defined as derivatives of the energy (or a suitably defined time-dependent quasi-energy), for example with respect to the presence of electric and magnetic fields, or nuclear positions, to name a few of the most important examples.

High-level correlated wave-function based ab initio computational methods have occasionally been applied to calculate properties of metal complexes. However, because of the scaling behavior of most of these methods with system size it is clear that the main tool for most of present-day computational coordination chemistry is density functional theory (DFT), both in its static version as applied to the electronic ground state (structures, energies) and in its time-dependent version (TD-DFT) as applied to determine excitation energies and dynamic properties. Consequently, the present article will focus on applications of DFT and TDDFT in the coordination chemistry field.

Ab initio computational chemistry of coordination compounds is a research field that has diversified to a point where it would be difficult to review most of the pertinent literature in a single article. A selection of reviews on more specialized topics is the following: Rosa et al. have reviewed the computation of excitation spectra of metal complexes [1]; Autschbach [2,3], and Autschbach and Ziegler [4–6] have reviewed computations of energy and many energy-derivative properties (NMR, EPR, optical, chiral, and others); Bühl, Kaupp, et al. have reviewed the computation of NMR in metal systems [7,8]; the results of experimental and computational NMR studies performed by Bagno et al. on systems containing ^{99}Ru, ^{103}Rh, ^{181}Ta, ^{183}W, and ^{199}Hg and $^{203/205}$Tl, among others, have been summarized by Bagno and Saielli [9]; and a number of researchers have reviewed computational work on EPR parameters of open-shell molecules in Ref. [10]; see for instance Neese's chapter on applications in bioinorganic chemistry [11]. A selection of reviews on a variety of topics including general aspects of transition metal complex modelling can be found, for example, in the February 2000 thematic issue of *Chem. Rev.* entitled "Computational Transition Metal Chemistry" and in a "Theoretical and Computational Chemistry" special issue of *Coord. Chem. Rev.* (vols. 238/239, March 2003). The modelling of reaction inorganic mechanisms has been reviewed, e.g., by Ziegler in Ref. [12]. For the field of magnetic resonance (both NMR and EPR), a book edited by Kaupp, Bühl, and Malkin, Ref. [10], provides a convenient collection of reviews (including some of the articles cited above) which contain many references to work on metal complexes. The "Chemist's Guide to Density Functional Theory" by Koch and Holthausen [13] quotes numerous benchmark data for structure, energy, reactivity, and optical and spectroscopic data obtained with DFT for metal complexes. A two-volume special issue of *Structure and Bonding* on "Principles and Applications of Density Functional Theory in Inorganic Chemistry" contains many references to original research articles dealing with coordination chemistry (vols. 112/113, 2004). It has already been pointed out that DFT has become the major theoretical tool to study metal complexes which is clearly reflected in the available reviews.

The present article is mainly concerned with recent advances made by the author and his collaborators in the first-principles modelling of NMR parameters and of the optical activity of transition metal complexes. It provides an account of topics presented by the author in a keynote lecture at the 37th International Congress of Coordination Chemistry that took place in Cape Town, South Africa, in August 2006. Some related studies by other research groups will also be discussed. The two research areas that are the subject of this article may seem only loosely connected at first sight, but it will be shown in Section 2 that their theoretical treatment is closely related. Specific studies of metal complexes and their main results will be discussed in Sections 3 and 4. Some general concluding remarks can be found in Section 5. Section 2 is not essential for reading Sections 3 and 4 and may be skipped, although this section provides some useful theoretical background.

2. Computation of linear response properties: a quick overview

A detailed overview of the theoretical approach to calculating so-called second-order properties (also termed linear response properties or double perturbation properties) of general molecules, with a focus on metal complexes, has been given by Autschbach and Ziegler in this Journal [4]. We summarize some of the main steps here but also extend upon the discussion of theoretical methods presented in Ref. [4]. The reader is referred to Refs. [4,14] for further details. We will restrict the discussion to the Born–Oppenheimer approximation, i.e. the nuclei are considered to be fixed and only the electronic degrees of freedom are included in the quantum mechanical formalism. Electromagnetic fields are treated semi-classically. Dimensionless atomic units with the electronic charge $e = 1$, electronic mass $m_e = 1$, Planck's constant $h = 2\pi$, $4\pi\epsilon_0 = 1$ and the speed of light $c \approx 137.036$ will be used throughout the theoretical section. Consequently, factors of $e, m_e, \hbar = h/(2\pi) = 1$ and $4\pi\epsilon_0$ will often be omitted in the equations. In these atomic units the fine structure constant α equals $1/c$. Boldface notation is used for vectors.

Definitions of molecular properties are related to the energy and the wavefunction via the system's Hamiltonian and the

Schrödinger (or Dirac) equation. Let $\hat{H}^{(0)}$ be a molecule's Hamiltonian in the absence of any electromagnetic fields, and

$$\hat{F}_i \cdot \cos(\omega_i t)\mathcal{F}_i \tag{1}$$

a set of fields that are able to perturb the electronic structure of the molecule, characterized by field strengths (amplitudes) $\mathcal{F}_i$, a frequency ω_i, and a perturbation operator $\hat{F}_i$ that depends only on spatial coordinates. The word "field" should not be taken too literally since the formalism is capable of describing a large variety of molecular perturbations. During the following discussion, as an illustrative example the reader should imagine a molecule subject to an oscillating external electric field such as from laser light. The definition (1) includes the case of static perturbations in the case that $\omega_i = 0$. For the moment we exclude possible cross terms $\hat{F}_{ij}$ between the fields.

Let $\hat{H}(\boldsymbol{\mathcal{F}}) = \hat{H}(\mathcal{F}_1, \mathcal{F}_2, \ldots)$ be the Hamiltonian for the "fully perturbed system", i.e. for the molecule under the influence of all fields present. The field amplitudes $\mathcal{F}_i$ serve as convenient perturbation-order parameters, i.e. the Hamiltonian can be expanded in a power series around $\boldsymbol{\mathcal{F}} = \mathbf{0}$ as

$$\hat{H} = \hat{H}^{(0)} + \sum_i \hat{H}^{(\mathcal{F}_i)}(\omega_i)\mathcal{F}_i + \ldots \tag{2a}$$

$$= \hat{H}^{(0)} + \sum_i \hat{F}_i \cdot \cos(\omega_i t)\mathcal{F}_i + \ldots \tag{2b}$$

where

$$\hat{H}^{(\mathcal{F}_i)}(\omega_i) := \left.\frac{\partial \hat{H}}{\partial \mathcal{F}_i}\right|_{\substack{\omega_i \\ \mathcal{F}_i = 0}} = \hat{F}_i \cdot \cos(\omega_i t) \tag{3}$$

Here and in the following the perturbation series notation:

$$A(x, y, \ldots) = A^{(0)} + A^{(x)}x + A^{(y)}y + A^{(xy)}xy + \ldots \tag{4}$$

is used where

$$A^{(0)} = A(x, y, \ldots)\Big|_{\substack{x=0 \\ y=0 \\ \cdots}};$$

$$A^{(x)} = \left.\frac{\partial A(x, y, \ldots)}{\partial x}\right|_{\substack{x=0 \\ y=0 \\ \cdots}}; \quad A^{(xy)} = \left.\frac{\partial^2 A(x, y)}{\partial x \partial y}\right|_{\substack{x=0 \\ y=0 \\ \cdots}}$$

etc. The quantity A can be a wavefunction, an energy, a property, an operator, depending on perturbations $x, y, \ldots$. In the example above, the perturbations are the field strengths $\mathcal{F}_i$. As already mentioned, for simplicity of notation we neglect for the moment any possible higher order terms in the Hamiltonian indicated by "$\cdots$" in Eqs. (2). The definition of $\hat{F}$ as a derivative of the Hamiltonian via the perturbation series may at first sight appear as an unnecessary complication in the formalism but it helps to keep track of the various derivative orders in terms other than the Hamiltonian. That is, the energy E and the electronic wavefunction Ψ of the molecule will be considered as perturbation series of the form (4) as well where – even if the Hamiltonian contains only first-order operators – the wavefunction- and energy-perturbation series will not terminate after first order in the field strengths. A complication in the notation arises due to the fact that the energy, for example, may depend not only explicitly on the perturbation parameters in the Hamiltonian but also implicitly via a dependence of the wavefunction on the perturbation. For simplicity we adopt here the partial-derivative notation for perturbation series that has been in use for a long time (see, e.g., Ref. [15]). The notation implies that in properties defined as energy derivatives any possible implicit dependencies on the perturbation via wavefunction parameters are included. Some authors have advocated for using a total-derivative notation where necessary [16]. Another way of avoiding notational ambiguities in a variational formalism has been suggested by King and Komornicki [17] which allows to retain a partial-derivative notation throughout.

Let us now consider a static molecular property F_1 described in quantum theory by its corresponding operator $\hat{F}_1$ and field amplitude $\mathcal{F}_1$. The expectation value of F_1 for the ground state with wavefunctions Ψ_0 is

$$F_1 = E^{(\mathcal{F}_1)} = \langle \Psi_0 | \hat{F}_1 | \Psi_0 \rangle \tag{5}$$

The designation of F_1 as a first-order energy perturbation $E^{(\mathcal{F}_1)}$ [same notation as in Eq. (4)] is in agreement with the Hellmann–Feynman theorem when considering our definition of $\hat{F}_1 = \hat{H}^{(\mathcal{F}_1)}$ for a static field and evaluating (5) at $\mathcal{F}_1 = 0$. We will always assume that the property F_1 is one of the electronic ground state and omit an index of "0" from the expectation value. The notation can be extended to perturbations of states other than the ground state. Further, in the absence of any perturbations the ground state shall be stationary and non-degenerate. An example for property F_1 is one of the Cartesian components (x, y, z) of the electronic dipole moment vector $\boldsymbol{D}$, for example D_x. The interaction Hamiltonian resulting from the molecule's dipole moment with an electric dipole field $\boldsymbol{\mathcal{E}}$ is given as $-\hat{\boldsymbol{D}} \cdot \boldsymbol{\mathcal{E}} = -(\hat{D}_x\mathcal{E}_x + \hat{D}_y\mathcal{E}_y + \hat{D}_z\mathcal{E}_z)$. In agreement with Eq. (5) the dipole moment component expectation values are the expectation values of the operators $\hat{D}_{x,y,z}$ obtained as the derivatives of the interaction Hamiltonian with respect to the field components (after removing the negative sign for reasons of consistency). In our notation, the perturbation operator $\hat{F}$ is the negative dipole moment operator for x, y, or z-direction, respectively, and the field strength $\mathcal{F}$ is the corresponding amplitude $\mathcal{E}_x$ (or y,z) of the external electric field.

Consider next a frequency-dependent perturbation field $F_2(\omega)$ described by the operator $\hat{F}_2 \cdot \cos(\omega t)\mathcal{F}_2$ just as in Eq. (1). We define the linear perturbation or linear response of property F_1 with respect to the perturbation $F_2(\omega)$ as the linear term in the expansion of F_1 as a perturbation series in the perturbing field's amplitude $\mathcal{F}_2$ around $\mathcal{F}_2 = 0$ as

$$F_1(\omega) = F_1^{(0)} + \left.\frac{\partial F_1}{\partial \mathcal{F}_2}\right|_{\substack{\omega \\ \mathcal{F}_2 = 0}} \mathcal{F}_2 + \mathcal{O}(\mathcal{F}_2^2) \tag{6a}$$

$$= F_1^{(0)} + F_1^{(\mathcal{F}_2)}(\omega)\mathcal{F}_2 + \mathcal{O}(\mathcal{F}_2^2) \tag{6b}$$

using the same notation as in (4). We identify the response function $\langle\langle \hat{F}_1; \hat{F}_2 \rangle\rangle_{-\omega}$ for property F_1 with respect to the perturbation

F_2 with the linear coefficient on the r.h.s. of (6b), i.e.

$$\langle\langle \hat{F}_1; \hat{F}_2 \rangle\rangle_{-\omega} = F_1^{(\mathcal{F}_2)}(\omega) = \left.\frac{\partial F_1}{\partial \mathcal{F}_2}\right|_{\substack{\omega \\ \mathcal{F}_2 = 0}} . \tag{7}$$

Since the molecular property F_1 is in turn a first derivative of the energy (Eq. (5)), the response function is a second derivative of the energy (or of the time-dependent quasi-energy in case that $\omega \neq 0$); also termed a bilinear or double perturbation of the energy of order $\mathcal{F}_1 \cdot \mathcal{F}_2$ in the field amplitudes. Eq. (7) relates the compact response function notation of Refs. [14,18] used by many theoretical chemists to the perturbation theory notation that we have adopted previously in Ref. [4]. By assuming the (hypothetical) knowledge of the exact ground state wavefunction Ψ_0 as well as all excited-state wavefunctions Ψ_j for the system at the expansion point where $\boldsymbol{\mathcal{F}} = \mathbf{0}$ (no fields), one can derive a sum-over-states (SOS) expression for the response function [4,18,19]:

$$\langle\langle \hat{F}_1; \hat{F}_2 \rangle\rangle_{\omega} = \sum_{j \neq 0} \left[\frac{\langle \Psi_0 | \hat{F}_1 | \Psi_j \rangle \langle \Psi_j | \hat{F}_2 | \Psi_0 \rangle}{\omega - \omega_j} - \frac{\langle \Psi_0 | \hat{F}_2 | \Psi_j \rangle \langle \Psi_j | \hat{F}_1 | \Psi_0 \rangle}{\omega + \omega_j} \right] . \tag{8}$$

Here, $\omega_j = (E_j - E_0)/\hbar$ is one of the excitation frequencies of the unperturbed system. The summation runs over all excited states. By assuming (without thereby imposing restrictions) that the wavefunctions for the unperturbed stationary states are all real, and considering the operators to be either purely real or purely imaginary, one obtains:

$$\langle\langle \hat{F}_1; \hat{F}_2 \rangle\rangle_{\omega} = 2 \sum_{j \neq 0} \frac{\omega_j \mathrm{Re}[\langle \Psi_0 | \hat{F}_1 | \Psi_j \rangle \langle \Psi_j | \hat{F}_2 | \Psi_0 \rangle]}{\omega^2 - \omega_j^2} \tag{9a}$$

if $\hat{F}_1$ and $\hat{F}_2$ are both real or both imaginary; or

$$\langle\langle \hat{F}_1; \hat{F}_2 \rangle\rangle_{\omega} = 2 \sum_{j \neq 0} \frac{\mathrm{i}\omega\, \mathrm{Im}[\langle \Psi_0 | \hat{F}_1 | \Psi_j \rangle \langle \Psi_j | \hat{F}_2 | \Psi_0 \rangle]}{\omega^2 - \omega_j^2} \tag{9b}$$

if $\hat{F}_1$ real and $\hat{F}_2$ is imaginary, or vice versa.

In the case that the Hamiltonian (2b) contains additional cross terms between the perturbing fields which we have not yet considered, for instance of the form:

$$\hat{F}_{i,j} \cdot \cos\omega_i \cos\omega_j \mathcal{F}_i \mathcal{F}_j, \tag{10}$$

then $\hat{F}_{i,j}$ is responsible for an energy term that is also bilinear in the field strengths. Consequently, for instance the perturbation $F_1^{(\mathcal{F}_2)}(\omega)$ would not only be given by the response function (7) but also by an additional expectation value of $\hat{F}_{1,2}$ calculated with the unperturbed wavefunction; i.e.

$$F_1^{(\mathcal{F}_2)}(\omega) = \langle\langle \hat{F}_1; \hat{F}_2 \rangle\rangle_{-\omega} + \langle \Psi_0 | \hat{F}_{1,2} | \Psi_0 \rangle \tag{11}$$

The unperturbed wavefunction has to be used in the second term on the r.h.s. of Eq. (11) because otherwise the expectation value would be of higher than bilinear order in the perturbing fields. An $\hat{F}_{1,2}$-term typically arises in the calculation of magnetic properties of molecules such as magnetizabilities, NMR chemical shifts and nuclear spin–spin coupling, and EPR parameters. For magnetic properties the response function contribution, i.e. the first term on the r.h.s. of (11), is usually called "paramagnetic" whereas the $\hat{F}_{1,2}$-term gives rise to the so-called "diamagnetic" contribution. Only the (paramagnetic) response-function contribution $\langle\langle \hat{F}_1; \hat{F}_2 \rangle\rangle_{\omega}$ is frequency-dependent. For perturbations involving electric fields there is usually no $\langle \Psi_0 | \hat{F}_{1,2} | \Psi_0 \rangle$ term. See Refs. [14,20,21] for details on obtaining the proper frequency-matching in (11) which were glossed over here for reasons of brevity.

The reader may wonder: what is the physical significance of the molecular property perturbation as defined in (11)? As an example, if $F_1 = D_x$, the x-component of the molecule's electronic dipole moment, and F_2 represent a perturbation by the y-component of an electric dipole field (perturbation operator $-\hat{D}_y$), then both perturbation operators $\hat{F}_1$ and $\hat{F}_2$ are real. There is no $\hat{F}_{1,2}$-term in this case. Consequently, $-\langle\langle \hat{D}_x; \hat{D}_y \rangle\rangle_{-\omega}$ in the form (9a) is the xy-component of the frequency-dependent dipole polarizability, $\alpha_{xy}(\omega)$, or of the static polarizability in the case that $\omega = 0$. In the time-domain, the perturbation of F_1 is in this case oscillating in phase with the perturbing field $F_2(t)$. As another example, let $F_1 = M_x$, a component of the molecule's magnetic dipole moment. If we consider a perturbation F_2 from $m_{\mathrm{A},y}$, the y-component of the spin-magnetic moment vector of nucleus A, then (9a) yields the paramagnetic part of the xy-component of the nuclear magnetic shielding tensor of nucleus A. In this case $\omega = 0$ and both perturbation operators are imaginary. There is also a diamagnetic term present in this case, i.e. the complete shielding tensor is calculated from a set of equations like (11), one for each component of the shielding tensor.

Let us consider next, as another example, the perturbation of a component of the molecule's electric dipole moment by a magnetic field. Maxwell's equations imply that a magnetic field can perturb the electric dipole moment of a molecule if it changes over time. Indeed, the time-dependent perturbation of the electric dipole by a magnetic dipole field is proportional to the time-derivative of the magnetic field [22]. In this case, $\hat{F}_1$ is real but $\hat{F}_2$ is imaginary, and the response is described by Eq. (9b) instead. The proportionality of the response to the time-derivative of the perturbing field can be seen from the factor of $\mathrm{i}\omega$ in the frequency-dependent response function (9b). The reader is reminded that Eqs. (9) describe the response in the frequency-domain, which is obtained from the time-dependent response by Fourier transformation. If $y(\omega)$ is the Fourier transform of a function $Y(t)$, then $\mathrm{i}\omega y(\omega)$ is the Fourier transform of $\mathrm{d}Y(t)/\mathrm{d}t$ [23]. Therefore, the factor of $\mathrm{i}\omega$ in (9b) indicates that the time-dependent response is proportional to the time-derivative of the perturbing field and implies that the perturbation of F_1 vanishes for static perturbations.

Let us return to the frequency dependent polarizability described by Eq. (9a), which is real. However, physically meaningful response functions (linear or nonlinear) are necessarily complex, i.e. they have a real and an imaginary part. Therefore, Eq. (9a) describes the real part α^{R} of a complex frequency-dependent polarizability $\alpha = \alpha^{\mathrm{R}} + i\alpha^{\mathrm{I}}$ (superscripts R and I indicate the real and imaginary part of the response function). The real and imaginary parts are related to each other by the

so-called Kramers–Kronig (KK) transformations [24,23]:

$$\alpha^R(\omega) = \frac{2}{\pi} \fint_0^\infty d\xi \cdot \frac{\xi \alpha^I(\xi)}{\xi^2 - \omega^2} \ , \tag{12a}$$

$$\alpha^I(\omega) = -\frac{2\omega}{\pi} \fint_0^\infty d\xi \cdot \frac{\alpha^R(\xi)}{\xi^2 - \omega^2} \tag{12b}$$

where $\fint$ indicates a principal-value integral. It is interesting to note that the KK transformations arise for purely mathematical reasons simply from requesting that the perturbation–response relationship is causal (no response before the perturbation takes place) and that the response function is "well behaved". The real part of the response function describes a refractive property (refractive index, optical rotation, etc.) whereas the imaginary part describes an absorptive property (electronic absorption spectrum, circular dichroism, etc.). Apart from a minus sign and the summation replaced by an integration, Eq. (12a) looks very similar to Eq. (9a) which, as we have seen, describes the linear response, for example, of the electric dipole moment to an electric field or similar cases where the operators $\hat{F}_1$ and $\hat{F}_2$ are both real or both imaginary. Consider an absorptive property $\alpha^{\mathrm{I}}(\omega)$ given by a set of "infinitely sharp" absorption lines centered at a set of excitation frequencies ω_j with generalized line strengths D_j, i.e. the line shape function is a Dirac delta function:

$$\alpha^{\mathrm{I}}(\omega) \sim \sum_j D_j \delta(\omega - \omega_j), \tag{13}$$

By substituting (13) into Eq. (12a) and considering that $\int_{-\infty}^{\infty} \mathrm{d}\xi f(\xi)\delta(\xi - \omega_j) = f(\omega_j)$ we obtain an expression similar to Eq. (9a) for α^{R} provided that the line strength is given by

$$D_j = \mathrm{Re}[\langle\Psi_0|\hat{F}_1|\Psi_j\rangle\langle\Psi_j|\hat{F}_2|\Psi_0\rangle] \tag{14}$$

It can be seen that in case of infinitely sharp absorption lines the real part of the response function, α^{R}, has poles at the excitation energies. The residues at the poles are equal to the quantities D_j, which represent the (generalized) line strengths for the absorptive property α^{I}.

In the case of electric-dipole–electric-dipole response (dipole moment perturbed by an electric field) the residues of the real part of the frequency-dependent polarizability calculated from (9a) are the dipole-strengths of the electronic absorption (UV–vis) spectrum. In the case of an electric-dipole–magnetic-dipole perturbation which is related to the optical rotation of a chiral molecule, the residues of the imaginary response function (9b) at the excitation energies are the rotatory strengths, which are the integrated intensities of the bands in the circular dichroism (CD) spectrum analogous to the way the dipole strengths are obtained from the absorption spectrum [25]. The response functions as defined here correspond only to one element of a second-rank response tensor. Most applications require a rotational averaging of the resulting tensor in order to extract the isotropic response and the isotropic line strengths needed to describe solution or gas phase measurements where molecules rotate freely. For dipole–dipole response tensors, this amounts to taking 1/3 of the sum of diagonal elements of the Cartesian 3×3 response matrix.

In the case of damping (through finite lifetime of excited states and other mechanisms) the spectral lines are not delta functions and the real part of the response assumes a smooth shape without actual divergencies. The derivation of Eq. (9) did not account for such damping mechanisms which is why there are singularities at the excitation energies. In the more realistic case where the absorptive property is described by

$$\alpha^{\mathrm{I}}(\omega) \sim \sum_j D_j \rho_j(\omega - \omega_j), \tag{15}$$

where ρ_j is a smooth normalized line shape function for excitation number j the line strength is still calculated from Eq. (14) but the SOS equation for α has to undergo a modification that reflects the presence of non-delta—like line shapes as the KK transforms of the ρ_j functions. Examples are discussed, for instance, in Barron's book [26] and in a recent article by Krykunov et al. [27].

In practice, the computation of response functions (refractive properties) or of the excitation energies and the residues of the response functions at the excitation energies (absorptive properties) rarely involve the explicit computation of excited states wavefunctions, i.e. the SOS equations are not applied directly. Instead, expressions for linear response functions are derived from considering analytic derivatives of static first-order molecular properties within a given approximate quantum chemical model (Hartree–Fock, coupled cluster, density functional theory (DFT), correlated perturbational schemes (Møller–Plesset, etc.)) and applying Eq. (7) or (11) directly. Typically, a resulting equation system is solved explicitly as a function of ω or, for direct calculations of the residues (for absorptive properties), transformed to an equation which allows to identify and calculate the poles and residues from an eigenvalue-type problem. In particular, the fact that in most quantum chemical computations a one-particle basis set is applied which may or may not depend explicitly on one of the perturbation parameters (field amplitudes) can – and should – be incorporated in the computational methods for linear or higher order response from the onset. The reader is referred to more specialized theoretical literature for further details [16,28,29].

Table 1 lists some of the molecular properties that can be computed with the formalism outlined so far. The list is to be understood as a sketchy overview only. For explicit expressions for the perturbation operators $\hat{F}_1$, $\hat{F}_2$, and $\hat{F}_{1,2}$ and an outline of how they are obtained within a quantum-theoretical framework we refer to Ref. [4]. In this earlier review we have also discussed a wide range of applications of theoretical methods to calculate these and other properties of transition metal complexes. It is clear from Table 1 that double perturbation/linear response theory provides access to a large number of the spectroscopic parameters of metal complexes that are relevant for day-to-day experimental work in coordination chemistry. As already mentioned, most of the more recent first-principles computations performed to date have employed density functional theory (DFT) because of its reasonable trade-off between accuracy and computational efficiency. The following sections will focus on some of the author's recent work in two of the areas

Table 1
A selection of second-order properties (linear response properties, double-perturbation properties) that can be calculated from Eq. (11), classified by pairs of perturbation parameters (actual or generalized field strengths) and frequency of the perturbation F_2 [a]

$\mathcal{F}_1$	$\mathcal{F}_2$	ω	SOS Eq.	Property	$\hat{F}_{1,2}$ term?
R_A	R_B	0	(9a)	Harmonic vibrations	No[b]
$\mathcal{E}$	$\mathcal{E}$	0 or $\neq$0	(9a)	Dipole polarizability, UV–VIS intensities, Dispersion coefficients for imag. ω	No
$\mathcal{E}$	R_A	0	(9a)	Infrared intensities	No
$\mathcal{E}$	$\mathcal{B}$	$\neq 0$	(9b)	Optical rotation and circular dichroism	No
$\mathcal{B}$	$\mathcal{B}$	0 or $\neq 0$	(9a)	Magnetic susceptibility	Yes
$\mathcal{B}$	m_A	0	(9a)	NMR chemical shifts	Yes
m_A	m_B	0	(9a)	NMR spin–spin coupling	Yes
$\mathcal{B}$	$\mathcal{S}$	0	(9a)	EPR g-tensor	Yes
m_A	$\mathcal{S}$	0	(9a)	EPR A-tensor	Yes

[a] $R_{A,B}$ = Nuclear position vector component (x, x, or z), nucleus A or B; $\mathcal{E}$ = electric dipole field vector component (x, y, or z); $\mathcal{B}$ = magnetic field vector component; m_A, m_B = component of nuclear spin magnetic moment vector; $\mathcal{S}$ = component of electron spin vector.
[b] Nuclear repulsion not included in electronic energy.

listed in Table 1 in more detail: NMR, and the computation of optical rotation and circular dichroism.

3. NMR computations

3.1. General considerations

The presence of spin magnetic moments $\boldsymbol{m}_A, \boldsymbol{m}_B, \ldots$ of nuclei A,B,... in a molecule is responsible for two of the basic parameters that define the outcome of the NMR experiment. These are the nuclear magnetic shielding tensor $\boldsymbol{\sigma}_A$ for nucleus A and the so-called indirect reduced coupling tensor K_{AB} for a pair of nuclei A, B. They yield the position of an NMR signal on the chemical shift scale, and its fine structure. Ab initio computations of the line shapes and widths are normally not carried out, i.e. the computations either simulate a hypothetical line spectrum or empirical broadening functions are applied in order to simulate the appearance of a real spectrum. Both $\boldsymbol{\sigma}_A$ and K_{AB} are second-rank tensors that can be defined via the phenomenological Hamiltonians:

$$H = -\boldsymbol{m}_A(1-\boldsymbol{\sigma}_A)\boldsymbol{\mathcal{B}}^{\text{ext}} \tag{16a}$$

for the shielding tensor and

$$H = \boldsymbol{m}_A \mathsf{K}_{AB} \boldsymbol{m}_B \tag{16b}$$

for the spin–spin coupling. As outlined in Section 2, the NMR chemical shifts of a metal complex can be calculated from static linear response functions involving the external magnetic field and one of the nuclear spin–magnetic moments. Since we have three Cartesian components of the $\boldsymbol{\mathcal{B}}$-field and three components of the nuclear magnetic moment vector one needs to calculate the nuclear magnetic shielding tensor $\boldsymbol{\sigma}$ for nucleus A in form of a 3×3 matrix as

$$\boldsymbol{\sigma}_A = \left.\frac{\partial^2 E}{\partial \boldsymbol{m}_A \partial \boldsymbol{\mathcal{B}}^{\text{ext}}}\right|_{\substack{\boldsymbol{m}_A = 0 \\ \boldsymbol{\mathcal{B}}^{\text{ext}} = 0}} \tag{17}$$

As outlined in Section 2, such a double derivative tensor of the energy can be calculated from a set of static linear response functions plus the associated diamagnetic parts, as in Eq. (11). The isotropic shielding constant σ the rotational average of the shielding tensor: $\sigma = (1/3)(\sigma_{xx} + \sigma_{yy} + \sigma_{zz})$. The chemical shift δ is determined as

$$\delta_A = \sigma^{\text{reference}} - \sigma_A \tag{18}$$

where $\sigma^{\text{reference}}$ is the shielding constant of a reference nucleus. Therefore, the calculation of chemical shifts makes use of a reference just like the experiment does. The reference can also be a hypothetical shielding related to a well-defined spectrometer frequency, as it is customary, for example, for ^{103}Rh NMR [30]. Computations are approximate; therefore it is sometimes of advantage to select a reference in the computations different from the experimental standard. Suppose we choose for the computation an alternative reference nucleus R with a shielding of σ_R and a chemical shift of $\delta_R = \sigma^{\text{reference}} - \sigma_R$ with respect to the standard reference, then:

$$\delta_A = \sigma^{\text{reference}} - \sigma_A = \sigma^{\text{reference}} - \sigma_A + \{\sigma_R - \sigma_R\} = \delta_A^R + \delta_R \tag{19}$$

where $\delta_A^R = \sigma_R - \sigma_A$ is the chemical shift for the nucleus of interest with respect to the alternative reference R. Often, R is chosen as chemically similar to the nucleus of interest, e.g. an atom with a similar oxidation state, similar bonding environment, and so on, and for δ_R the experimental value is used. This way, a maximum amount of error cancellation can be achieved in the computation. In computational studies with larger sets of metal complexes it is also possible to avoid the computation of a problematic reference by fitting calculated shieldings to experimental shifts and extracting a reference shielding from the fit where $\delta^{\text{expt.}} = 0$, as was done, for example, by Bühl et al. for ^{99}Ru [31].

For calculations of nuclear magnetic spin–spin coupling, one needs to evaluate the reduced indirect spin–spin coupling tensor:

$$\mathsf{K}_{AB} = \left.\frac{\partial^2 E}{\partial \boldsymbol{m}_A \partial \boldsymbol{m}_B}\right|_{\substack{\boldsymbol{m}_A = 0 \\ \boldsymbol{m}_B = 0}} \tag{20}$$

which is, like the corresponding expression for the shielding tensor, in formal agreement with the phenomenological Hamil-

tonian (16b). We will not consider here additional contributions from the dipolar coupling which averages to zero for freely rotation molecules (solution NMR measurements). Measured J-couplings are related to the rotational average of the $\mathbf{K}$coupling tensor as

$$J_{AB} = \frac{\hbar}{2\pi}\gamma_A\gamma_B K_{AB} \tag{21}$$

with $K = (1/3)(K_{xx} + K_{yy} + K_{zz})$ being the rotational average of the $\mathbf{K}$tensor. The γs are the nuclear magneto-gyric ratios.

It should be pointed out that chemical shifts δ and indirect nuclear spin–spin coupling constants K are response properties of the electronic system. The measurement obviously relies on the presence of nuclear spins but the computational result is not dependent on the magnitudes of the nuclear spins, or on the spin quantum numbers. Therefore, in the "clamped nucleus" approximation chemical shifts calculated for different isotopes of the same element are identical. Isotope effects on chemical shifts and other response properties can be obtained computationally from considering vibrational corrections. If calculated J-coupling constants are reported, then obviously the value depends on the isotopes via the magneto-gyric ratios (Eq. (21)) whereas the indirect couplings K are not isotope-dependent (except, again, via vibrational corrections).

3.2. Relativistic effects

An important aspect of calculations of NMR parameters of heavy metal complexes is the strong influence of relativistic effects. "Heavy" means here typically elements with nuclear charges around 50 or higher. The fact that relativistic effects are responsible for much of the chemical behavior of heavy elements has become textbook knowledge. We refer to some of the available review papers on relativistic theoretical NMR methods for methodology details and comprehensive literature surveys [2,32]. In a nutshell, high nuclear charges have a strong impact on the shape of the valence orbitals in heavy element systems. In order to understand why high nuclear charges are related to relativistic effects consider the following qualitative argument [33–35]: the ground state (1s) energy of an electron bound to a nucleus of charge $+Z$ is $E = -Z^2/2$ atomic units. The kinetic energy is calculated as $T = -E = +Z^2/2$. Since kinetic energy is 1/2 mass times velocity squared and the electron mass equals one atomic unit, in a classical system we would have an average electron velocity $v = Z$ atomic units. In these units the speed of light has a rather small numerical value, $c = 137.036$ only. That is, for heavy nuclei the electron velocities may approach a substantial fraction of the speed of light which causes significant effects from special relativity, which are of order $v^2/c^2 = Z^2/c^2$. Trends for chemical shifts and J-coupling are caused by chemical influences, i.e. by the valence orbitals. Interestingly, not only core orbitals are affected by relativistic effects but also, to the same order Z^2/c^2, valence orbitals [34]. Therefore NMR parameters are affected by relativistic effects. Moreover, NMR parameters are heavily influenced by near-nucleus features of the valence orbitals due to the locality of the operators involved [4]. Here, relativistic effects are also largest which is the reason why NMR parameters are much stronger affected by relativistic effects than, for example, the energy, geometries, or many other spectroscopic parameters [32] (i.e. they are of order Z^2/c^2 but the prefactor is large). As a consequence, there are substantial relativistic ("heavy atom" HA) effects on chemical shifts of light atoms (LA) in their neighborhood (HALA [36] effects), relativistic effects on the chemical shift of the heavy atom itself (a HAHA [36] effect), and sometimes extremely large relativistic terms on the order of 100% of the nonrelativistic value or even greater in J-coupling constants involving at least one heavy nucleus. Experience gathered so far from computations indicates that HALA effects on J-couplings between light nuclei are often of minor importance, although this may not be the case if the coupling is mediated by the metal's valence shell. Relativistic effects can be subdivided into spin-free (scalar) contributions and those due to spin-orbit coupling. The HALA effect on chemical shifts as well as a substantial portion of the HAHA effect on chemical shifts results from spin-orbit coupling via a mechanism that causes the external magnetic field to induce a spin-polarization in the molecule. For spin–spin coupling, where the transfer of electronic spin-polarization through bonds is typically the dominant mechanism, spin-orbit effects tend to be small unless the J-coupling involves two heavy p-block elements [37,38]. Scalar relativistic effects must not be neglected in the study of spin–spin coupling when heavy nuclei are involved. This review does not specifically focus on relativistic effects but it should be kept in mind that NMR computations on complexes with heavier metals or heavy-atom ligands should normally involve some type of relativistic theory.

As already mentioned, the following selection of recent NMR computations on systems containing metals does not represent a comprehensive overview. The reader is referred to the literature cited in the Introduction for topics not covered here.

3.3. Pt–Tl bonded systems

Le Guennic et al. have studied the metal NMR parameters of a set of non-buttressed Pt–Tl bonded systems $[(NC)_5Pt–Tl(CN)_n]^{n-}$, $n = 0, 1, 2, 3$ (**1**–**4**) and the related system $[(NC)_5Pt–Tl–Pt(CN)_5]^{3-}$ (**5**) synthesized by Glaser et al. [39,40] and two bridged amidate complexes **6** and **7** synthesized by Matsumoto et al. [41,42] and model systems based thereupon. See Fig. 1. The chemical shifts of some of these systems will be discussed in a separate section. We focus here on the metal–metal J-coupling constants. Data reported here refers to the isotopes ^{195}Pt and ^{205}Tl. An earlier computational investigation by Autschbach and Ziegler had suggested that at least 50% of the huge magnitude of the Pt–Tl coupling constant of the $n = 1$ system (expt.: 57 kHz) is due to coordination of Tl by solvent molecules (water) [43]. Computations on the whole series **1**–**4** as well as complex **5** showed that solvent coordination effects on $^1J(^{195}Pt–^{205}Tl)$ of the $n = 0$ system (**1**) are even larger [42,44], changing the gas phase result of about −10 kHz into a solution result of about +55 kHz in computations that differed only by the absence or presence of solvent. It was also found that both explicit solvent molecules and bulk solvent effects need

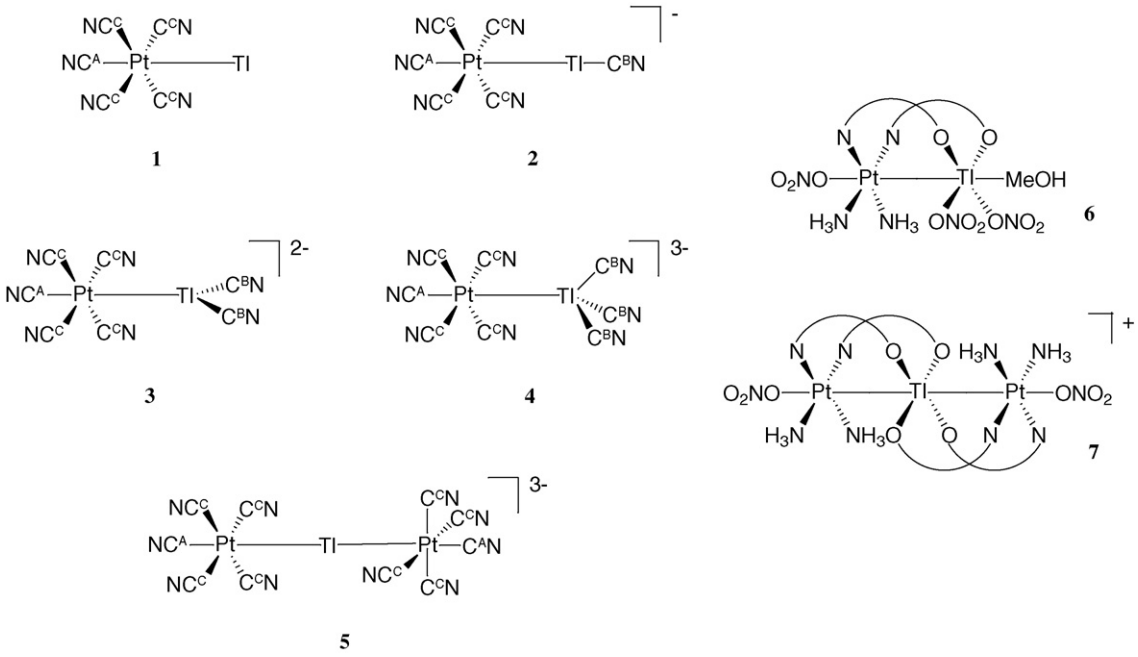

Fig. 1. Structures of various Pt–Tl bonded complexes (**1**–**7**).

to be included in the computations on **1**–**4** in order to obtain the same trend for $^{1}J(^{195}\mathrm{Pt}–^{205}\mathrm{Tl})$ as found experimentally, and that the simultaneous application of both an a continuum solvent model (the COnductor-like Screening MOdel, COSMO [45,46]) and an asymptotically correct DFT exchange-correlation potential (SAOP [47,48]) is beneficial. The main computational results obtained by Autschbach and Le Guennic [44] are displayed in graphical form in Fig. 2. For model "C", very good agreement with experiment was obtained. Results for the metal–ligand coupling constants for these systems have also been reported in Ref. [44], with similar success of the solvation model. The Tl–C coupling constants are very strongly influenced by the solvent coordination, whereas the Pt–C coupling constants are less affected, although some improvement is obtained from considering solvent effects. Solvent coordination had previously also been found to be responsible for the unintuitive relative magnitudes of $^{1}J(^{205}\mathrm{Tl}–^{13}\mathrm{C})$ and $^{2}J(^{205}\mathrm{Tl}-{}^{13}\mathrm{C})$ for complex **2** [43], with the latter being more than 3 times larger than the former.

The findings from the theoretical investigation of metal–metal and metal–ligand coupling constants in **1**–**5** can be briefly summarized as follows: (i) The trend for $^{1}J(^{195}\mathrm{Pt}–^{205}\mathrm{Tl})$ along the series is caused by solvent coordination, mainly by direct coordination of the Tl atom. In gas phase or a weakly coordinating solvent, $^{1}J(^{195}\mathrm{Pt}–^{205}\mathrm{Tl})$ for **1**–**4** would exhibit the opposite trend. (ii) In computational modelling of heavy metal NMR parameters a reasonable description of the experimental trends requires to include at least one explicit solvation shell in case the metal has open coordination sites, and at least a continuum solvation model to estimate the effects of a second, third, …, solvation shell. Reproducing trends for different solvents might require further refinement of the model (see below). The importance to fill the metal's first coordination sphere with solvent molecules has also been highlighted in computations on other heavy-atomic systems [49,50]. It was found reassuring that the computational protocol yielding best agreement with experiment for $^{1}J(^{195}\mathrm{Pt}–^{205}\mathrm{Tl})$ also yielded the best agreement with experiment for metal–ligand couplings as well as for the metal chemical shifts (to be discussed below).

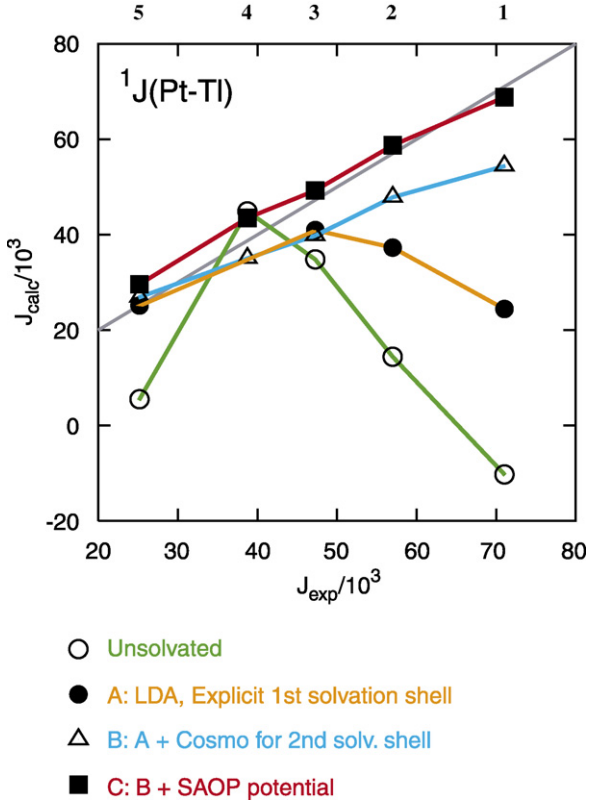

Fig. 2. $^{1}J(^{195}\mathrm{Pt}–^{205}\mathrm{Tl})$ for complexes **1**–**5**, calculated vs. experimental data [44]. The straight line indicates where $J_{calc} = J_{exp}$. Solvent is water. COSMO is a continuum solvent model. Non-hybrid DFT computations.

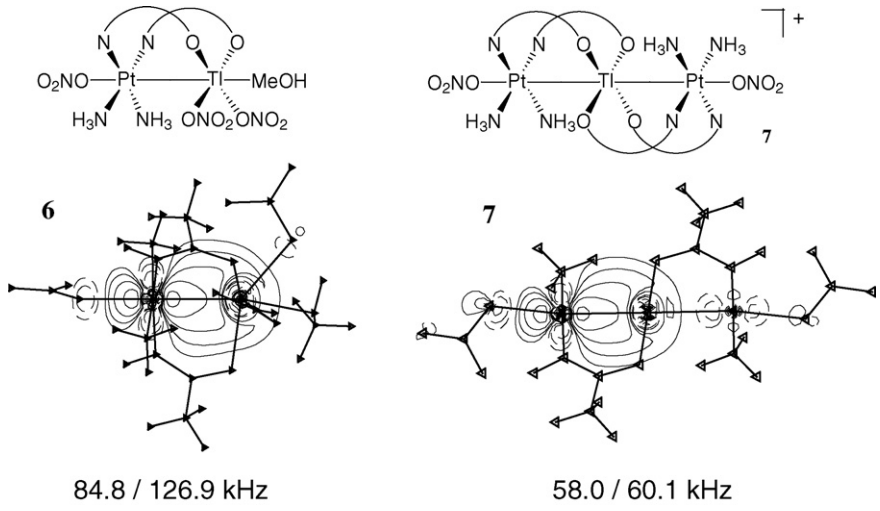

Fig. 3. Contribution from Pt–Tl σ-bond orbitals to $^{1}J(^{195}\mathrm{Pt}–^{205}\mathrm{Tl})$ for complexes **6** and **7** (Fermi-contact term only, no solvent effects included, contrib. from orbital/total FC term) [41,42]. The σ-bonding orbital is considerably delocalized along the molecular axis. The axial ligands have therefore a strong influence on $^{1}J(^{195}\mathrm{Pt}–^{205}\mathrm{Tl})$.

Unfortunately, the computational protocol that led to nearly quantitative agreement with experiment for $^{1}J(^{195}\mathrm{Pt}–^{205}\mathrm{Tl})$ of **1**–**5** turned out to significantly overestimate the Pt–Tl coupling constants in the amidate-bridged complexes **6** and **7** shown in Fig. 1[51]. As an example, the record-large $^{1}J(^{195}\mathrm{Pt}–^{205}\mathrm{Tl})$ of 146.8 kHz of **6** was calculated as 159.6 kHz when using the COSMO solvation model (gas phase calculation: 114.2 kHz) but this good agreement with experiment was only achieved without using the asymptotically corrected SAOP potential. With SAOP and COSMO applied simultaneously, the computations yielded 221.7 kHz for $^{1}J(^{195}\mathrm{Pt}–^{205}\mathrm{Tl})$ in spin-free relativistic calculations. Calculations including spin-orbit coupling yielded 172.9 kHz (COSMO) and 236.8 kHz (COSMO + SAOP), respectively. For **7**, the experimental $^{1}J(^{195}\mathrm{Pt}–^{205}\mathrm{Tl})$ is 88.8 kHz. The computations yielded 80.6 kHz (COSMO) and 105.5 kHz (COSMO + SAOP) with spin-free relativistic DFT, respectively. The spin-orbit results were 87.9 and 113.3 kHz. The trends regarding the computational model and the sign of the spin-orbit corrections are the same for both complexes. Whereas the inclusion of the asymptotic correction in the functional yielded a welcome but relatively minor increase of $^{1}J(^{195}\mathrm{Pt}–^{205}\mathrm{Tl})$ for **1**–**5**, complexes **6** and **7** turned out to be very sensitive to the computational model. Le Guennic, Matsumoto, and Autschbach have analyzed the situation in detail [42] and traced this sensitivity back to small metal 6s-contributions in low-lying unoccupied σ-orbitals that change considerably, percentage-wise, depending on the computational model. These orbitals describe the electronic spin-polarization in the system due to the presence of the nuclear spins and are therefore vital for the calculation of the coupling constants (the reader is reminded that the coupling constant is calculated from a set of response functions which involve both occupied and unoccupied orbitals). It is likely that quantitative agreement between theory and experiment for complexes such as **6** and **7** will only be achieved with a very high-level computational model since their sensitivity leaves little room for error suppression/compensation.

It is interesting to note the drastic differences in the Pt–Tl coupling constants between **6** and **7** and among the series **1**–**5**. Le Guennic et al. employed existing, and developed a range of new, analysis tools for spin–spin coupling constants for the study **6** and **7** [42] (see also some educational applications to organic molecules as described in Ref. [52]). Fig. 3 shows the contributions of the metal–metal σ-bonding localized orbitals (contributions from the dominant Fermi-contact term only, no solvation model applied) to $^{1}J(^{195}\mathrm{Pt}–^{205}\mathrm{Tl})$ of **6** and **7**. In both cases the orbitals are significantly delocalized along the complexes' long axis which rationalizes the strong influence in particular of the ligands *trans* to the metal–metal bond. The large differences between $^{1}J(^{195}\mathrm{Pt}–^{205}\mathrm{Tl})$ for **6**, **7**, **1** and **2**, for instance, can to a large extent be traced back to the σ-coordinating ability of this axial ligand. The stronger this coordination, the smaller the metal–metal coupling—a *trans*-effect. The same mechanism also causes Pt–Pt coupling constants to vary by an order of magnitude [53], and Hg–Hg coupling constants to stay well below an upper theoretical estimate of almost 1 MHz calculated for $[\mathrm{Hg–Hg}]^{2+}$ [50].

3.4. Metal chemical shifts, in particular of ^{195}Pt

^{195}Pt is one of the heaviest NMR nuclei. Techniques for detecting the nuclear magnetic resonance of ^{195}Pt have been developed quite early [54,55]. Pt NMR has since become a powerful tool to study the chemistry of Pt complexes [56]. A large set of experimental data are available for the benchmarking of relativistic theoretical NMR methods that were developed during the past decade [37]. However, surprisingly few attempts have yet been made to calculate Pt chemical shifts from first principles. Most of the available studies reported difficulties with reproducing experimental data to a satisfactory degree.

As an example, the first DFT investigation of Pt chemical shifts performed by Gilbert and Ziegler [57] on *cis* and *trans* PtX_2Y_2 systems with $X = \{\mathrm{Cl, Br, I}\}^{-}$ and $Y = \{\mathrm{Cl, Br, I}\}^{-}$ or $\{SMe_2, NH_3, PMe_3, AsMe_3\}^{+}$ yielded a RMS deviation of

about 300 ppm between theory and experiment for a set of 24 complexes. The overall agreement with experiment is in fact quite good considering that the chemical shift range of these compounds spans about 3400 ppm. However, one of the compounds, $PtCl_2(SMe_2)_2$, had to be chosen as the NMR reference in order to obtain this agreement with experiment, in the spirit of Eq. (19). In the experiments, the Pt reference is usually a solution of Na_2PtCl_6 in water which is not easy to model computationally. Indeed, Gilbert and Ziegler already hinted in their paper at the difficulties of modelling the NMR parameters of charged complex ions in coordinating polar solvents.

The main results of Gilbert and Ziegler's computational study are typical for metal chemical shifts [2]: often, explanations of trends for chemical shifts among similar compounds are sought in terms of trends regarding the HOMO–LUMO gap, which in turn can be related to Eq. (9a) which describes the paramagnetic shielding tensor elements (there is a similar equation for the DFT and Hartree–Fock (HF) nuclear shielding involving orbital energies instead of the total energies of Eq. (9a), although generally the orbital energy differences do not have to be related to the excitation energies). The argument is that a large energy-separation between occupied and unoccupied orbitals causes the paramagnetic component of the nuclear shielding to be small (large denominators). However, in metal complexes the trends are often opposite what would be expected based on the magnitude of the HOMO–LUMO gap because the matrix elements in the numerator of (9a) and its HF or DFT analogs may yield opposite trends. This is also what Gilbert and Ziegler found for their set of Pt chemical shifts. The balance between the trends was termed "delicate", which means it is not easy to estimate qualitatively without performing a computation. Similar findings had previously been reported by Wolff and Ziegler for ^{13}C shifts in 5d transition metal carbonyls [58]. Overall, Gilbert and Ziegler found that qualitative rules for Pt shifts based on hard-soft acid–base concepts, namely that softer ligands yield more negative Pt shifts, were reproduced in the computations and caused by trends in the paramagnetic part of the shielding tensor from spin-free and spin-orbit terms of the same sign.

Autschbach and Le Guennic studied the metal chemical shifts of the Pt–Tl bonded complexes **1**–**7** which were already discussed in the preceding section. See Fig. 1. During the course of a computational study of the Pt and Tl chemical shifts of **1**–**5** [59], pronounced difficulties were noted in obtaining agreement with experimental data for the Pt shifts in these complexes when using the standard experimental reference $[PtCl_6]^{2-}$ (**8**) in the computations. Better agreement with experiment was obtained when using the complex $[Pt(CN)_6]^{2-}$ (**9**) as a reference which was attributed to the higher similarity of the ligands in **7** compared to **1**–**5**. The authors also suspected problems with the density functional which they considered more severe in **8** than in **9** due to the smaller HOMO–LUMO gap in **8**. As can be seen from Eq. (9a) for the response function in the static case ($\omega = 0$), if for some reason the functional underestimates the HOMO–LUMO gap this leads to an overestimation of the paramagnetic terms in the shielding tensor (the HOMO–LUMO gap serves as a zero-order estimate for the excitation energy in "pure" (non-hybrid) density functional theory [28]). It appeared that the paramagnetic spin-orbit terms in **8** were excessively large although other sources of error in the computations could not be ruled out. Overall, the best agreement with experiment was obtained when using complex **4** as an internal computational reference which again hinted at problems of modelling Pt chemical shifts. Even with complex **4** as the reference, computed solvent effects on the Pt and Tl chemical shifts were found to be very large, which emphasizes again the necessity of modelling solvent effects (here: water) in transition metal NMR computations. The data shown in Fig. 4 supports the main conclusion of the computational study: as a minimal requirement the computations need to include explicit solvent molecules to fill the first coordination sphere of the metals as well as a model for outer solvation shells at least in form of a continuum model (COSMO was used for the computational study reported in Ref. [59]). Otherwise, deviations of up to several thousand ppm between computations and experiment might be obtained for the metal chemical shifts, even when using one of the complexes as the NMR reference. It can also be seen that the explicit first solvation shell – which merely completes the

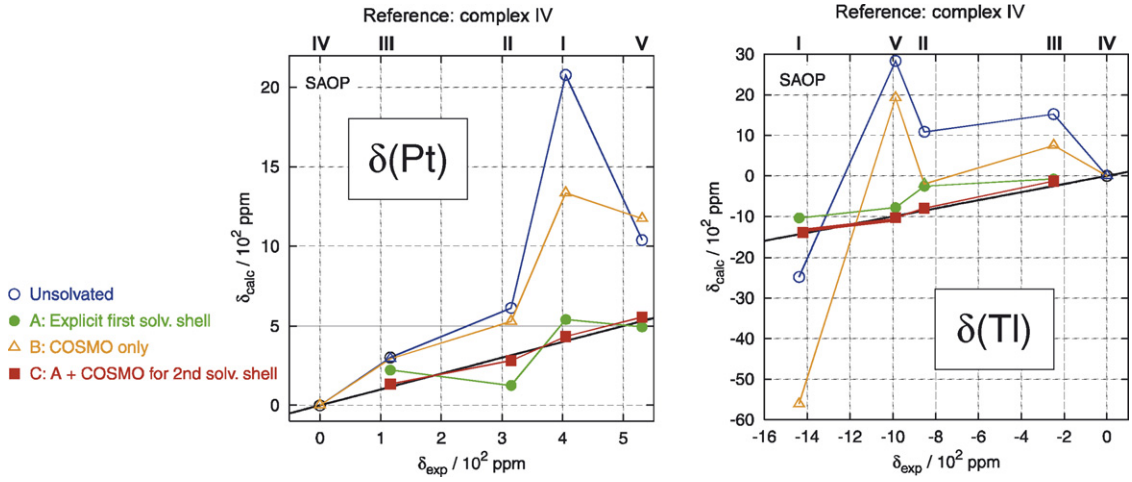

Fig. 4. ^{195}Pt and ^{205}Tl chemical shifts of the complexes **1**–**5** shown in Fig. 1, from Ref. [59]. Calculated versus experimental shifts. The straight line indicates where $\delta_{calc} = \delta_{exp}$. Solvent is water. COSMO is a continuum solvent model.

first coordination sphere around Tl for this set of complexes – yields reasonable agreement with experiment whereas the application of a continuum model without explicit solvation does not perform satisfactorily. Unfortunately, as for the *J*-couplings, the computational model that worked best for **1**–**5** did not yield satisfactory agreement with experiment for the chemical shifts in a follow-up study of the complexes **6** and **7** [42].

In 2005, Fowe et al. reported excellent agreement between computations and experiment of the Pt chemical shifts for the series $[PtCl_{6-n}Br_n]^{2-}$, n= 0–6 (**8**, **10**–**15**). The authors applied a very similar computational "pure DFT" method as used by Gilbert and Ziegler [57], and by Autschbach and Le Guennic [59,42]. Fowe et al. also noted a strong sensitivity of the Pt chemical shift with respect to Pt-ligand bond lengths. It was verified by calculations on $[PtCl_6]^{2-}$ and $[PtBr_6]^{2-}$ using a continuum solvent model that solvent-induced structural changes have a strong impact on the calculated Pt shielding constants. Since the first coordination sphere of the metal in the $[PtCl_{6-n}Br_n]^{2-}$ series is already occupied by regular ligands one might expect a similar performance of the computational model as found by Autschbach and Le Guennic for **1**–**5** (the computations used similar functionals, basis sets, and relativistic operators), which was indeed the case. Recently, Koch et al. investigated the Pt NMR chemical shifts of a variety of Pt^{IV} species including the $[PtCl_{6-n}Br_n]^{2-}$ (n = 0–6) and $[PtCl_{5-n}Br_n(H_2O)]^{-}$ (n = 0–5) series as well as species with hydroxy ligands experimentally and computationally [60,61]. The computational approach was similar to those used in the other DFT studies discussed so far. Excellent agreement with experiment and the correct trends for ligand substitution were obtained in this work. Very systematic trends upon ligand substitution found experimentally and verified by computations allowed to identify a number of previously unidentified species as well as the identification of various geometrical isomers. Despite that the complexes under scrutiny were chemically quite similar and that the set contained the experimental standard reference, the results obtained by Fowe et al. and by Koch et al. are encouraging. If deficiencies in the density functionals or the chosen "ZORA" relativistic method [62] would cause ligand effects on the metal shifts to be grossly over- or underestimated this would potentially have surfaced in these studies.

These implications regarding the principle performance of the density functionals prompted Sterzel and Autschbach to investigate Pt chemical shifts in solution for a set of complexes with different oxidation state, and different coordination and solvation spheres [63]. The purpose of this work was to eliminate some of the potential fortuitous error compensation that arises when comparing chemical shifts among a series of similar compounds, and to test in particular the modelling of solvation effects. The complexes **8**, **16**, and **17** were chosen, see Fig. 5. In addition to static computations, Born–Oppenheimer molecular dynamics simulations (BOMD) were also performed on **8** and **16**. It turned out to be rather challenging to compute the chemical shift of **16** with respect to the standard Pt reference **8**. As a main result of the study it was concluded that previous computations on **1**–**15** did not employ a flexible enough basis set, neither for the metal nor for the ligands, and that error compensation masked this important factor. Another issue was the modelling of unspecific solvent effects for which some explicit solvation in conjunction with molecular dynamics simulations appeared to be necessary. The chemical shifts and spin–spin coupling constants for **1**–**5** and the chemical shifts of octahedral Pt^{IV}-species with respect to **8** as the reference were not overly strongly affected by basis set truncation and approximations in

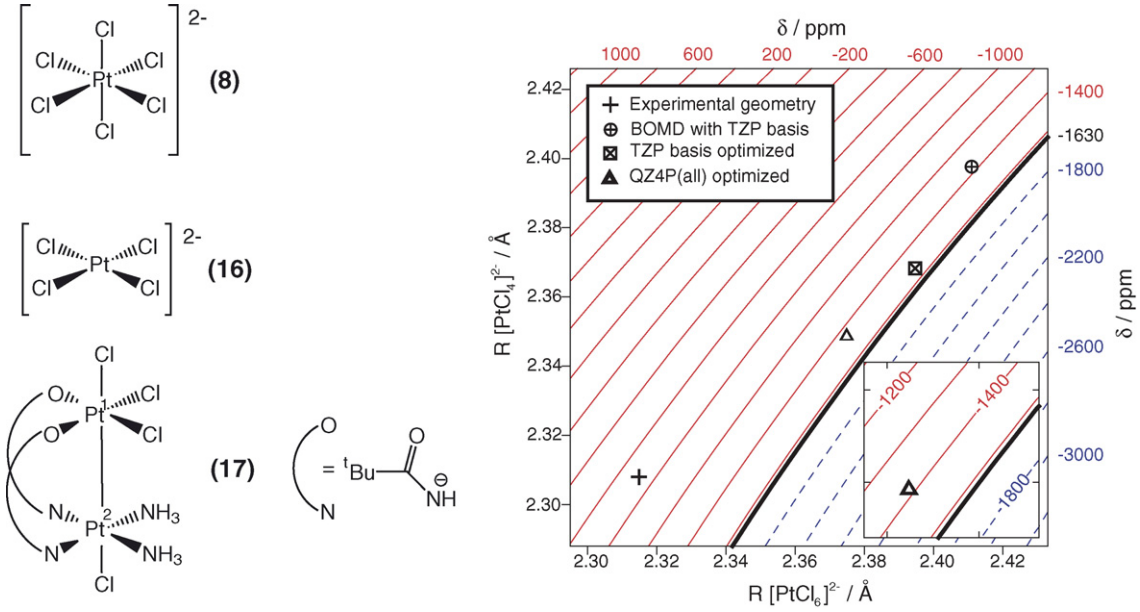

Fig. 5. Left: molecules used for the ^{195}Pt-shift benchmark computations reported in Ref. [63]. Right: dependence of the $[PtCl_4]^{2-}$ chemical shift (reference: $[PtCl_6]^{2-}$) on the Pt–Cl bond distances in the probe and the reference complex. Chemical shift surface calculated with QZ4P basis for Pt and TZP basis on remaining atoms (short: QZ4P(Pt)). Inset: surface calculated with QZ4P on all atoms. Solid thin lines indicate where the calculated shift is larger in magnitude, dashed thin lines where the shift is smaller in magnitude than the experimental value of −1630 ppm (solid thick line). The markers indicate the optimized/average geometries obtained with the method listed in the key and the resulting QZ4P(Pt) chemical shift (inset: QZ4P).

the solvent model, but the difficulties with complexes **6** and **7** and other Pt species can likely be attributed to these approximations. By comparison of static with BOMD computations it was found that the best performing static computational model, yielding −1528 ppm for the Pt chemical shift of **16** compared to the experimental value of −1630 ppm, still benefited from error compensation. This model used a more flexible basis than previous studies (QZ4P instead of TZP or TZ2P), but only for the metal not for the ligands. This basis set was termed QZ4P(Pt) in Ref. [63]. A trade-off between truncating the basis set and treating the solvent–solute interactions approximately was found to be one of the major factors. Sterzel et al. argued that similarly good agreement between theory and experiment may be obtained if the NMR chemical shifts are computed with a highly flexible basis set on all atoms from molecular-dynamics averaging including a large number of explicit solvent molecules. Fig. 5 shows the dependence of the chemical shift of **16** on the Pt–Cl bond distances in **16** and the NMR reference **8**. Neighboring contour lines differ by 200 ppm. This strong geometric dependence of the chemical shift requires either an essentially correct dynamic treatment of metal, ligands, and solvation shells, or at least a computational model in which the error compensation regarding geometric effects and solvent–solute interactions is balanced and well understood (i.e. one either attempts to obtain the much sought-after "right answer for precisely the right reasons" or at least a "good-enough answer for good enough reasons" that are well understood and where approximations are acceptable). The more affordable static QZ4P(Pt) + COSMO model was tested on complex **16**: the chemical shifts for Pt^1 and Pt^2 were calculated as 475 and −1216 ppm (all computations including effects from spin-orbit coupling) which compare acceptably well with the experimental shifts of 512 and −1023 ppm [64]. The findings regarding the pronounced sensitivity of the Pt chemical shifts with respect to geometric parameters in particular for negatively charged species are in line with results obtained by Bühl et al. from molecular-dynamics studies on 3d transition metal complexes, for example of Fe [65,66] and Co [67]. In summary, it appears that in Pt chemical shift calculations issues with density functional are perhaps less pronounced than previously thought [42,59] but that modelling of the complex structure and solvation is even more critical than indicated by some of the earlier work on Pt chemical shifts. Ref. [63] highlights in particular the importance of the portion of unspecific solvent effects that is not well described by a continuum solvation model (e.g. hydrogen bonding).

The recipe of adding one explicit shell of solvent molecules in static computations, along with approximating further solvent shells by a continuum model, has been applied by Autschbach and Zheng to compute solvent effects on ^{99}Ru chemical shifts for *fac*-$[Ru(CO)_3I_3]^-$ [68]. Because of the large chemical shift range of approximately 18,000 ppm reported so far for ^{99}Ru [69], even comparatively small differences in structure and bonding can result in sizeable chemical shift changes. Therefore, ^{99}Ru NMR represents a stringent test for computational models. Computations of ^{99}Ru chemical shifts had previously been performed by Bühl et al. [31], Bagno and Bonchio [70,71], and Ooms and Wasylishen [69]. As part of their solvation study, Autschbach and Zheng have also re-investigated the performance of various computational models and in particular the importance of relativistic effects for a benchmark set of different Ru complexes. It was found that (i) Relativistic effects are of relatively minor importance for Ru chemical shifts (and likely for chemical shifts of other 4d metals) although their inclusion improves agreement with experiment. (ii) The choice of the density functional is important. Hybrid functionals perform somewhat better for Ru chemical shifts. Among the considered complexes approximations in the functionals appeared to affect the standard reference ($[Ru(CN)_6]^{4-}$ in aqueous solution) most strongly. (iii) The trends for the ^{99}Ru chemical shift of *fac*-$[Ru(CO)_3I_3]^-$ in different solvents (acetone, acetonitrile, chloroform, methanol, NMP (*N*-methyl-pyrrolidinone), pyridine, sulfolane, and water) were reproduced in the computations to a similar degree as ligand trends among a set of different Ru complexes. (iv) Neither just a continuum model nor just a few solvent molecules were sufficient for reproducing the trend; both were required. This was initially surprising since *fac*-$[Ru(CO)_3I_3]^-$ does not have open coordination sites at the metal; the solvent effects are therefore rather unspecific. However, these findings support the conclusions regarding unspecific solvent effects drawn for Pt chemical shifts. (v) Benchmark results for a range of Ru complexes with different ligands appear to be indicative of the performance of the same level of theory to reproduce rather unspecific solvent trends in the calculations, and vice versa.

3.5. Gold cages

Relativistic NMR computations on cage-structures formed by heavy metal atoms have been performed recently. As an example, Pyykkö et al. predicted, among a variety of other optical and spectroscopic parameters, the ^{183}W chemical shift and Au–Au spin–spin couplings in WAu_{12} [72]. This species was theoretically predicted by Pyykkö et al. to be stable for reasons of strong relativistic effects, a perfect 18-electron bonding, and aurophilic attraction [73]. Subsequently, WAu_{12} was detected in mass-spectrometry experiments. [74] In a follow-up computational study [72] the W nucleus in the center of the icosahedral Au_{12} cage was predicted to be exceptionally strongly shielded, resulting in a chemical shift of about −13, 000 ppm with respect to the reference WO_4^{2-}. To our knowledge experimental data are not yet available in order to confirm this finding. The authors found that relativistic effects represent only a secondary contribution to this extraordinarily large shielding (most notably a contribution of 3850 ppm from spin-orbit coupling which exceeds the largest spin-orbit shielding found in an earlier DFT benchmark study of ^{183}W shifts by a factor of two [75]). The most important influence was found to be a strong paramagnetic shielding of the external field by the Au cage. The reduced W–Au and Au–Au spin–spin coupling constants were also computed. For K (W–Au) the spin-free relativistic result was 7350×10^{19} T^2 J^{-1} compared to a nonrelativistic value of 3322×10^{19} T^2 J^{-1}. The magnitude of this relativistic increase appears to be typical for couplings between two heavy atoms [2] although it does by no means represent the ceiling of relativistic effects for coupling between two metals with 6s valence shells. As an example,

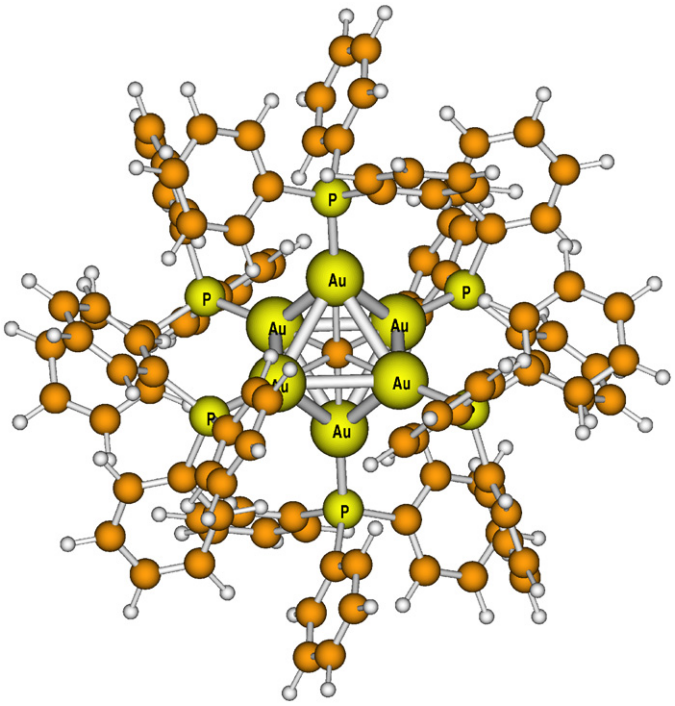

Fig. 6. Optimized structure of $[(Ph_3PAu)_6C]^{2+}$ (**18**), from Ref. [76]

the average of one- to three-bond Au–Au couplings in WAu_{12} was calculated as $12{,}365 \times 10^{19}\ T^2\ J^{-1}$ relativistically, but only $2459 \times 10^{19}\ T^2\ J^{-1}$ nonrelativistically.

The carbon atom inside an Au_6 cage can be used as a probe for the electronic structure of the gold gage in the fascinating complex $[(Ph_3PAu)_6C]^{2+}$ (**18**) shown in Fig. 6. The complex was synthesized by Schmidbaur et al. in 1988 and extensively investigated by single crystal X-ray diffraction and NMR spectroscopy. [77,78]. In interstitial carbides ^{13}C nuclei are known to be very strongly deshielded. Known examples are, for instance, the ^{13}C NMR chemical shift of a series of interstitial carbides in transition-metal clusters [79–83]. On the other hand, we have seen that tungsten nucleus in WAu_{12} is exceptionally strongly shielded from the external magnetic field due to the surrounding gold cage. One may therefore expect the interstitial ^{13}C NMR chemical shift in **18** to be large in magnitude, either positive or negative, depending whether the chemical environment is more similar to carbides or more similar to clusters like WAu_{12}. Previous analyses of the electronic structure of main-group-element-centered octahedral gold clusters have highlighted the differences between **18** and interstitial carbide complexes [78,84]. In particular, the gold systems are thought to have radial C–Au bonds and rather weak (aurophilic) interactions between the Au-phosphine ligands, whereas in the case of interstitial carbide complexes strong metal–metal bonds stabilize the structures [85–87]. For a derivative of **18**, the complex $[C\{Au[P(C_6H_5)_2(p\text{-}C_6H_4NMe_2)]\}_6]^{2+}$ (**19**), Schmidbaur et al. unambiguously assigned a signal at $\delta = 137.27$ ppm to the interstitial carbon atom [88]. Knowing the chemical shifts and coupling constants for **19**, the authors identified a weak ^{13}C signal at $\delta = 135.2$ ppm in the parent complex **18** as originating from the interstitial carbon. The ^{13}C resonance of this carbon atom therefore appeared in a completely unexpected region. A computational study of these systems by Le Guennic et al. [76] concluded that the suppression of strongly shielding spin-orbit contributions from the Au cage due to electronic effects from the phosphine ligands is responsible for the unexpected chemical shift of the central carbon in **18** and **19**. Without the phosphine ligands, a "naked" Au_6^{2+} cage would indeed cause the carbon nucleus inside to be very strongly shielded. The calculated chemical shift was about −303 ppm with respect to TMS, mostly due to spin-orbit coupling terms in the shielding tensor (this strong HALA effect is similar to the "normal halogen dependence" of carbon and proton shifts [5,32]). With the strongly σ-coordinating phosphine ligands present, the spin-orbit terms of the cental carbon's shift in **18** and **19** are almost completely quenched and a chemical shift in the aromatic region results. The mechanism that suppresses the spin-orbit terms is probably the same that causes metal–metal and metal–ligand *J*-couplings to decrease if a strongly σ-bonding ligand is added *trans* to the bond that transfers the *J*-coupling [76]. This mechanism can be understood in relatively simple terms: a σ-binding *trans*-ligand (axial ligand) most effectively reduces the s-character of the metal–metal or metal–ligand bond for which the *J*-coupling is considered [2,50,53]. The HALA spin-orbit contribution to nuclear shielding is similar to the dominant Fermi-contact spin-mechanism of *J*-coupling [32,89]; therefore similar effects from *trans* ligands may be expected.

3.6. Poly-oxo metallates

A number of computational studies have appeared recently focussing on NMR chemical shifts of metal and hetero atoms in poly-oxo-metallates (POM). Poblet, Kazansky, et al. considered ^{17}O and ^{183}W chemical shifts for a set of poly-oxo-tungstanates [90], among them $[W_6O_{19}]^{2-}$, $[CH_3OTiW_5O_{18}]^{3-}$, $[W_5O_{18}W^{II}NO_3]^-$, $[W_{10}O_{32}]^{4-}$, α–δ–γ-$[XW_{12}O_{40}]^{n-}$ with X = As,Ga,Ge,P,Si,Al,B, β-$[PW_9O_{28}Br_6]^{3-}$, $[P_2W_{18}O_{62}]^{6-}$, $[PW_2O_{14}]^{3-}$, and $[W_7O_{24}]^{6-}$. The number of truly heavy atoms in some of these systems is seen to be very large by ab initio computational chemistry standards, making the computation of their NMR parameters a daunting task. Spin-orbit computations, which are particularly demanding, were facilitated to some extent by speed-ups implemented by the author [91] in the relativistic DFT NMR program of Wolff and Ziegler [62]. For small W complexes Ziegler et al. had previously fund very good correlation between theory and experiment, with the slope of a linear fit of calculated versus experimental ^{183}W shifts near unity [75]. In their POM study, Poblet, Kazansky, et al. also found a good linear correlation between experimental and calculated ^{183}W shifts. However, the slope of the fit line was only 0.785 which was tentatively attributed to the basis sets that had to be employed in order to keep the computational effort manageable [90] and – a related issue – to the quality of the optimized structures. For the ^{17}O shifts a much better slope of 1.06 was obtained. Overall, the structure-NMR trends for these POMs were satisfactorily reproduced. A reliable assignment of the POMs' structure by a comparison of computations with experiment was deemed reliable only in the case of

widely separated NMR shifts. The authors also hinted at the need for including solvent effects for POMs with large q/m (charge-to-mass) ratio.

In a follow-up study [92], Poblet, Kazansky, et al. focussed on the reduced poly-oxo-tungstanates $[W_5O_{18}W^{II}NO]^{3-}$, γ-$[SiW_{12}O_{40}]^{6-}$, $[P_2W_{18}O_{62}]^{8-}$, and $[W_{10}O_{32}]^{6-}$, using similar computational methods as applied in Ref. [90]. In comparison with the oxidized forms, it was found that overall the computations described the chemical shift changes upon reduction well, although large discrepancies between some of the calculated shifts and experiments were noted, in particular for $W_5O_{18}W^{II}NO^{3-}$. These discrepancies were attributed to problems with the density functional describing the interaction between W^{II} and the NO ligand.

Bagno et al. have recently performed a study of ^{183}W shifts in tungsten POMs [93] including solvent effects, using relativistic all-electron DFT methods [62,91]. Previous work by Bagno and Bonchio employed effective core potentials [94]. See also Ref. [9]. Bagno et al. reported in Ref. [93] a computational study of several POM's belonging to various structural groups: Lindqvist ($[W_6O_{19}]^{2-}$, $[VW_5O_{19}]^{3-}$, $[V_2W_4O_{19}]^{4-}$), Anderson ($[W_7O_{24}]^{6-}$, $[TeW_6O_{24}]^{6-}$), α-Keggin ($[BW_{12}O_{40}]^{5-}$, $[PW_{12}O_{40}]^{3-}$, $[SiW_{12}O_{40}]^{4-}$, $[GeW_{12}O_{40}]^{4-}$) and decatungstates ($[W_{10}O_{32}]^{4-}$, $[W_{10}O_{32}]^{6-}$); see Fig. 7 for an example of the structures that were computed. As for other NMR computations on POMs [90,92], the large number of heavy atoms made the computational study very challenging. A focus here has been the consideration of solvent effects by means of the COSMO model. The best agreement was obtained at the highest computational level which included solvent effects and spin-orbit coupling. Despite the rather narrow chemical shift range of the sample set (about 500 ppm) as compared to the 8000 ppm shift range found overall for ^{183}W the computations performed very satisfactorily; see Fig. 7 for an overview. The average deviation was 35 ppm or only about 7% of the shift range considered. The largest deviations seen in Fig. 7 were found for species with large q/m or q/A (charge-to-surface area ratio) where inclusion of solvent effects also had the strongest impact, highlighting once more the importance of modelling the chemical environment of metal systems for the purpose of NMR computations. The small intercept of the calculated-versus-experimental shift correlation was possible because one of the POMs, $W_6O_{19}^{2-}$, was selected as the NMR reference. The absolute errors with respect to the standard reference WO_4^{2-} would have been larger but this is, of course, inconsequential for the all-important trends and likely rather highlight difficulties with the modelling of WO_4^{2-} in solution (large q/A). Inclusion of solvent effects systematically improved the results, both directly in the NMR computations as well as through application of the solvent model in the geometry optimizations, which tended to cause some shrinkage of the POM structures. The authors concluded that such computations might indeed become a valuable aid in structural assignments of POMs by NMR.

3.7. H–D coupling in dihydrogen and hydride complexes

The *J*-coupling between hydrogens in dihydrogen and hydride metal complexes has been of interest to chemists for a long time [95]. The coupling between proton and deuterium has been found useful to determine the H–H distance in such complexes and to classify them accordingly as a dihydrogen complex, a hydride, or "in between" (i.e. as an elongated dihydrogen complex or a compressed hydride). See Fig. 8 for an illustration. Consequently, such complexes have attracted the interest of theoreticians. For example, *J*(H–D) was computed by Hush et al. [97,98] for a set of osmium complexes. The authors found a strong correlation between the calculated *J*(H–D) and the strength of the Os–H_2 interaction as well as a correlation between *J*(H–D) and the H–D internuclear distance in the complexes. Gusev considered a large set of complexes with widely varying H–H distances and found that hybrid DFT computa-

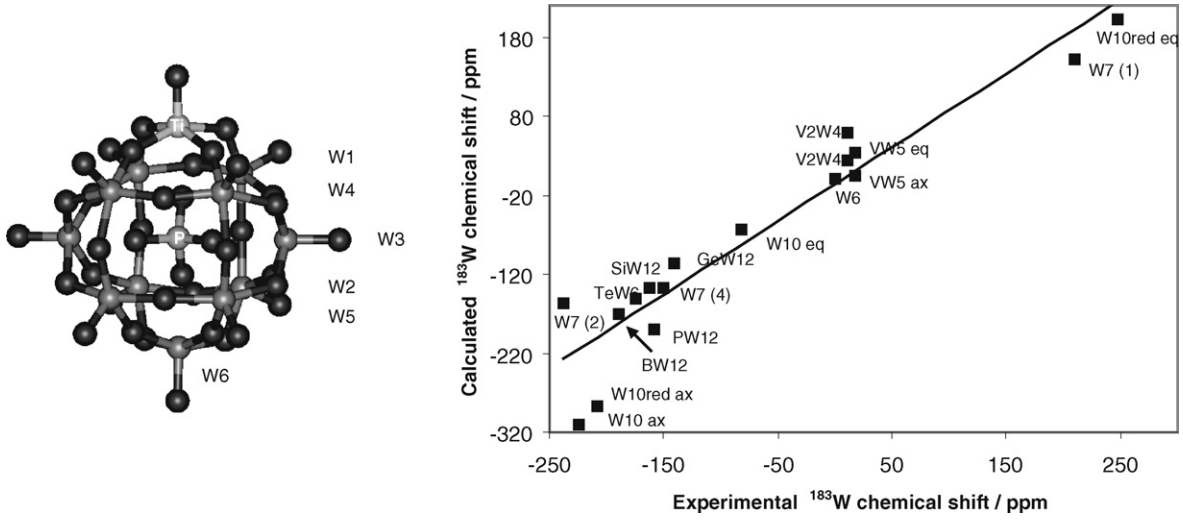

Fig. 7. Left: structure of $[PW_{11}TiO_{40}]^{5-}$ as an example of the poly-oxo-metallates (POM) studied by Bagno et al., Ref. [93]. Right: correlation between calculated and experimental ^{183}W chemical shifts relative to $[W_6O_{19}]^{2-}$ in various POM. All-electron spin-orbit DFT computations; COSMO solvation model for water. The correlation line has a slope of 0.93, intercept −7 ppm.

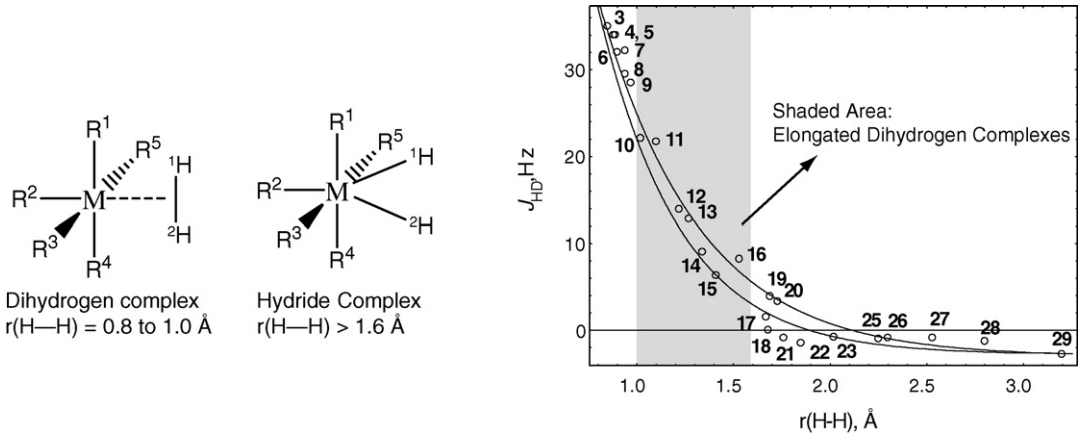

Fig. 8. Dihydrogen and dihydride metal complexes can be classified by the distance between the hydrogens. The number of ligands may vary depending on the metal. The ^{1}H–^{2}H nuclear spin–spin coupling (J(H–D)) is very strongly dependent on the distance between the hydrogens, as seen in the right figure, courtesy of Prof. D. Gusev, Wilfried Laurier University, Canada (modified by the author). A similar figure was originally published in Ref. [96]. Correlation between H–D coupling and H–H distance according to two fits, see Ref. [96] for details and numbering of the complexes.

tions reproduced the overall trend quite well, although relative (percentage) errors were sometimes substantial [96]. In a subsequent study, Le Guennic et al. determined on a set of 14 heavy metal complexes that spin-orbit coupling does not represent a strong HALA influence on the H–D couplings [99]. Therefore, meaningful conclusions can be drawn from scalar relativistic DFT computations on such systems, for instance by using a scalar relativistic pseudopotential for the metal. The study by Le Guennic et al. also confirmed Gusev's finding that the H–D couplings for the complexes with largest H–H distance are negative. They should be viewed as two-bond couplings mediated the H–metal–H bonds.

One of the main drawbacks of the theoretical studies cited so far in this section has been the neglect of vibrational corrections on the H–D couplings. Since the two lightest atomic nuclei are involved in this coupling, vibrational corrections and tunneling effects can be substantial. For free dihydrogen, the zero-point vibrational correction of J(H–D) is on the order of 2.2–2.8 Hz [99,100] which represents roughly 5% of the experimental coupling of 42.9 ± 0.1 Hz for the HD isotopomer [101]. In computational (usually DFT) studies of the NMR of metal complexes, improving the results by a 5% correction would be desirable but not vital. The large coupling constants for dihydrogen complexes with H–H distances close to free dihydrogen fall into this category. However, for two reasons one may expect that for elongated dihydrogen and compressed hydride complexes the relative importance of vibrational corrections to J(H–D) to exceed the 5% calculated for free dihydrogen. The first reason lies in the strong dependence of J(H–D) on the H–D distance. A neglected 2–3 Hz correction of a small H–D coupling constant found in elongated dihydrogen complexes or hydrides with large H–H distances can render a computational analysis of J(H–D) questionable or even useless. Second, in the interesting regime where the H–D bond is still (partially) intact but severely elongated, strong anharmonicity of the potential energy surface (PES) can potentially cause larger (absolute) vibrational corrections as found in free dihydrogen. An assessment of DFT methods to verify empirical relationships for J(H–D) as a function of the H–H distance should therefore include vibrational averaging.

Mort and Autschbach have recently performed such a study on a set of six heavy metal complexes [102]. Four of them, **20**–**23**, are shown in Fig. 9. Vibrational averages of a molecular property P can be calculated to lowest order in an expansion

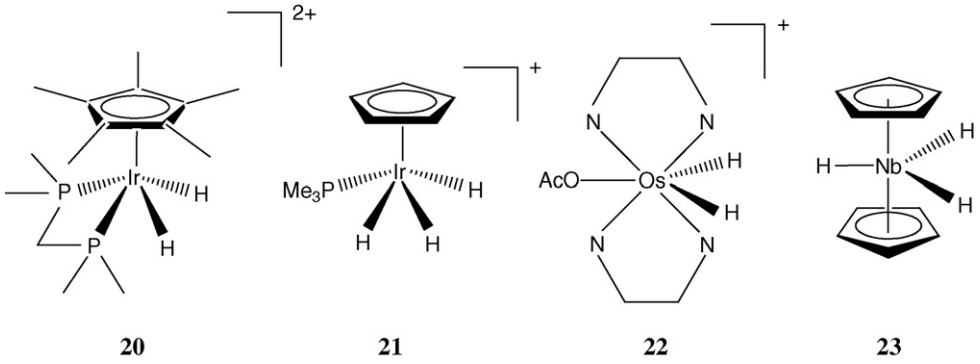

Fig. 9. Some complexes for which J(H–D) was computed as a function of temperature, see Ref. [102].

around the value P_e obtained for the equilibrium structure as

$$\langle P\rangle_T = P_e - \frac{1}{4}\sum_i \frac{1}{\hbar\omega_i}\left(\frac{\partial P}{\partial q_i}\right)\sum_j \coth\left(\frac{\hbar\omega_j}{2kT}\right)k_{ijj} + \frac{1}{4}\sum_i \coth\left(\frac{\hbar\omega_i}{2kT}\right)\left(\frac{\partial^2 P}{\partial q_i^2}\right) \quad (22)$$

where T is the temperature, ω_i the fundamental vibrational frequency of normal mode number i with dimensionless normal coordinate q_i, and k_{ijj} is one of the cubic force constants [29,102–104]. The expression also yields a vibrationally averaged structure by considering as P the set of nuclear coordinates in the system. Using this expression with $P = J$(H–D) and calculating the derivatives in Eq. (22) by finite differences, Mort and Autschbach found substantial zero-point corrections on the order of several Hz for complexes **20**–**23**. For **21**, a moderate temperature-dependence of J(H–D) was also predicted which is yet to be confirmed by experiment. Unfortunately, the somewhat smaller calculated T-dependence for the experimentally available J(H–T) coupling over the experimentally accessible temperature range is within the experiment's uncertainties [105].

For **22** and **23**, the predicted temperature-dependence of J(H–D) was small but for very different reasons. Complex **22** has a very anharmonic PES along the H–H stretch coordinate which yielded a zero-point vibrationally averaged J of 10.9 Hz as compared to a 6.7 Hz equilibrium value (expt.: 9 Hz at 233 K). Clearly, the vibrational correction must not be ignored. However, a cancellation of anharmonicity corrections (the k_{ijj}-terms in Eq. (22)) and the property-curvature terms ($\partial^2 P/\partial q_i^2$ in Eq. (22)) led to a negligible temperature-dependence of the vibrational corrections. On the other hand, for the hydride **23** with an experimental J(H–D) of −0.9 Hz (sign assigned based on computational data [96,102]), the PES is quite harmonic, the zero-point vibrational corrections are small, and the T-dependence is negligible because of the harmonicity of the PES. The H–H stretch coordinate does not play a role here anymore because the H–D coupling in this hydride complex with large H–H distance (the expt. estimate is 1.76(9) Å) is mediated by the H–metal–H bonds.

Complex **20** is a particularly interesting case. Experiments [106] reported a very strong temperature-dependence of J(H–D) in this this "compressed dihydride" which was supported by computational work performed by Lluch, Lledos, et al. based on calculations of the nuclear wavefunctions in a two-dimensional subspace of the PES and averaging the corresponding J-surface [107]. See Fig. 10, the "Literature" curve represents the computed results by Lluch, LLedos, et al. from Ref. [107]. The reason for the strong temperature-dependence is seen in the double-minimum PES sketched in Fig. 10, as pointed out in Ref. [107]. By simply using the zero-point averaged J-couplings calculated separately for each minimum, Mort and Autschbach obtained a comparable temperature-dependence from a Boltzmann average of the two couplings ("Literature reconstructed") as did Lluch, Lledos et al. from quantum dynamics [107]. As temperature increases, the minimum at short H–H distance becomes populated. This minimum has a much higher J(H–D) than the dihydride structure. An even better agreement with experiment was obtained when zero-point vibrational corrections were also included in the Boltzmann factors and when low-lying vibrational modes neglected by Lluch, Lledos, et al. [107] were considered in the computations (see the $\langle J\rangle_B$ curve in Fig. 10).

Based on computations of the temperature-dependence of J(H–D) based on Eq. (22) Mort and Autschbach predicted in Ref. [102] that the Re complex **24** shown in Fig. 11 should have a measurable T-dependence of J(H–D). Such a temperature-dependence should arise for this complex not because of a double-minimum potential but because of a strong anharmonicity of the PES, resulting in temperature-dependent anharmonicity and property-curvature vibrational corrections that do not cancel (in contrast to complex **23**). The magnitude of the temperature-dependence as shown in Fig. 11 was subsequently confirmed by Gusev [108] (the experimentally determined coupling constants are between 12.75 and 13.07 Hz). We note in passing that the coth-factors in Eq. (22) have a very similar T-dependence as the shape of the $J(T)$-function in Fig. 11. For further details and a discussion of a complex where the low-order property-expansion around the equilibrium geometry is too "near-sighted" in order to yield the temperature-

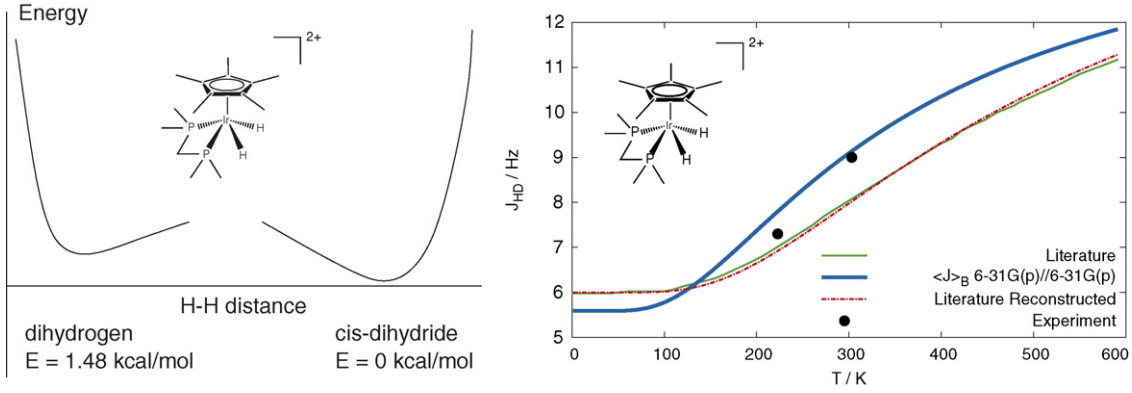

Fig. 10. Left: sketch of the potential energy surface of $[Ir(dmpm)Cp^*H_2]^{2+}$ (**20**) along the H–H internuclear distance, from Ref. [102]. The barrier height was not calculated. Right: Boltzmann average of the zero-point vibrational average of the spin–spin coupling constant at the *cis*-dihydride and dihydrogen minima of complex $[Ir(dmpm)Cp^*H_2]^{2+}$, hybrid DFT computations [102]. Experimental data indicated by black circles, Ref. [106]. See text for details.

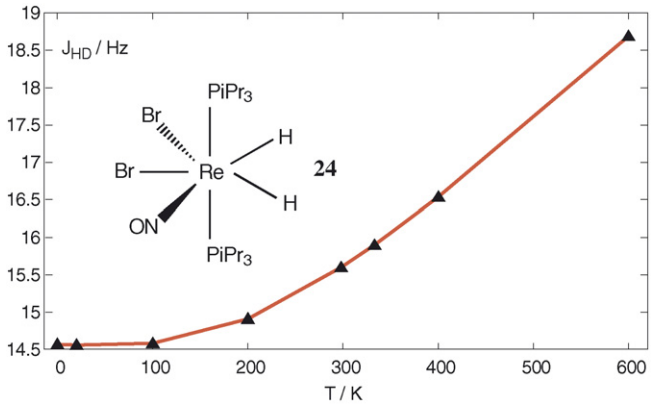

Fig. 11. Structure of the Re complex **24**, and computed temperature dependence of J(H–D). The increase of J between 25 and 60 °C is in agreement with experimental data recently obtained by Prof. D. Gusev [108]. Hybrid DFT data taken from Ref. [102].

dependence of J(H–D) we refer the reader to Ref. [102] and references cited therein.

4. Computation of the optical activity of transition metal complexes

4.1. General considerations

As already indicated in Section 2, optical activity-related observables can be obtained from computations of linear response functions or their residues where one of the fields is a time-dependent magnetic field. We restrict the discussion to electronic optical activity and refer the reader to Ref. [4] for further details regarding vibrational optical activity and references to computational studies on metal complexes. Using Buckingham's notation [109], an element of the mixed electric-magnetic dipole polarizability tensor G' is the linear response function:

$$G'_{\alpha,\beta}(\omega) = -\mathrm{Im}\langle\langle \hat{D}_\alpha; \hat{M}_\beta \rangle\rangle_\omega \tag{23}$$

where $\hat{D}_\alpha$ and $\hat{M}_\beta$ are Cartesian components of the one-electron electric and magnetic dipole moment vector operators $\hat{\boldsymbol{D}}$ and $\hat{\boldsymbol{M}}$, respectively. Since $\hat{\boldsymbol{D}}$ is real and $\hat{\boldsymbol{M}}$ is imaginary the SOS form of the G'-tensor elements is given by Eq. (9b) multiplied with $+i$. The G'-tensor vanishes for zero frequency. The isotropic optical rotation parameter $\beta(\omega)$ for a chiral molecule is related to the rotational average of G' by

$$\beta(\omega) = -\frac{1}{3\omega} \sum_{\alpha=x,y,z} G'_{\alpha,\alpha}(\omega) \tag{24}$$

Although G' vanishes at zero frequency, because of the division by the frequency β has a non-vanishing zero-frequency limit (as long as the molecule is chiral). This limit is readily obtained from the SOS Eq. (9b) of G' after division by ω as [110]:

$$\beta(0) = \frac{1}{3} \sum_{\alpha=x,y,z} \mathrm{Im}\langle \Psi^{(\mathcal{E}_\alpha)} | \Psi^{(\mathcal{B}_\alpha)} \rangle \tag{25}$$

by employing SOS expressions for the first-order terms in the perturbed wavefunctions (see Ref. [4] for explicit expressions). $\Psi^{(\mathcal{B}_\alpha)}$ for static fields is also an ingredient for the computation of NMR chemical shifts, or EPR g-tensors. The computation of optical activity affords some unique challenges, however, since the time-dependent nature of the perturbing fields may expose additional deficiencies of the computational approximations (e.g. in density functionals [28]).

The optical rotation parameter β arises in a theoretical treatment of molecule-light interactions when considering the difference in the refractive index of a medium for left- and right-handed circularly polarized light [22,25,111]. This difference is precisely what causes the phenomenon of optical rotation since a linearly polarized light beam can be decomposed into a left- and right-hand circularly polarized component with the plane of polarization defined by the phase shift between the circular components. If the refractive index is not the same for the circularly polarized components, as it is the case in a chiral medium, this causes a phase shift between these components, resulting in the plane of polarization of the linearly polarized beam to rotate as it passes through the medium. For the typical case of a solution of chiral molecules in a nonchiral solvent, the molecules are freely rotating and the rotation angle is proportional to the isotropic optical rotation parameter, the cuvette length, and the concentration of the chiral molecules. Experimental data are typically reported as the specific rotation $[\alpha]$ in degrees per weight-concentration in (g/cm^3) and per dm of cuvette length at a given wavelength λ or wavenumber $\tilde{\nu} = 1/\lambda$. It is obtained from β calculated for a chiral molecule as

$$[\alpha]_{\tilde{\nu}} = 28,800 \cdot \frac{\pi^2 N_A \tilde{\nu}^2}{M} \beta(\tilde{\nu}), \tag{26}$$

with N_A being Avogadro's number, M the molecular weight in g/mol, and $\tilde{\nu}$ in cm^{-1} (or λ in cm). The optical rotation parameter β is here in commonly used c.g.s. units of cm^4. The molar rotation $[\phi]_\lambda$ is another frequently used quantity, with $[\phi]_\lambda = [\alpha]_\lambda(M/100)$. Eq. (26) excludes local field corrections. In computations they can be added, for instance by employing a continuum solvation model similar to those discussed in the NMR part of this paper, or explicit solvent molecules, or both, which has the benefit of including solvent–solute interactions on the ground state geometry and electronic structure as well.

As in the case of the polarizability discussed earlier, the derivation of (9b) did not consider any damping for the excited states and describes the real part of a complex response function. The imaginary part of the complex optical rotation parameter $\beta(\omega)$ describes the differential absorption of circularly polarized light, also termed circular dichroism (CD). A similar argument as used previously for relating the electronic absorption spectrum to the imaginary part of the frequency-dependent polarizability can be used to derive the CD analogs of the absorption line strengths, the rotatory strengths R_j, as

$$R_j = \mathrm{Im}\left[\langle \Psi_0 | \hat{\boldsymbol{D}} | \Psi_j \rangle \cdot \langle \Psi_j | \hat{\boldsymbol{M}} | \Psi_0 \rangle \right] \tag{27}$$

for the transition from the ground state to state j. The scalar product of the transition dipole moment vectors is taken in Eq.

(27). Some broadening is always present in experimental spectra and the real and imaginary part of the complex optical rotation parameter are both smooth functions of the wavelength or frequency. The rotatory strengths are related to the integrated intensity of the experimentally observed CD signal $\Delta\epsilon$, the difference in the absorption coefficient for left- and right-hand circularly polarized light, as

$$R_j = \text{const.} \int_{\text{CD Band}\,j} \frac{d\tilde{\nu}}{\tilde{\nu}} \frac{\Delta\epsilon(\tilde{\nu})}{l/(\text{mol cm})} \tag{28}$$

The constant of proportionality in the last equation is approx. $22.97 \times 10^{-40}\text{esu}^2\,\text{cm}^2$, in c.g.s. units in which the rotatory strengths are usually reported. Another measure of CD is the ellipticity $[\theta]$ of the outgoing light beam in an optical rotation experiment. The ellipticity is directly proportional to $\Delta\varepsilon$ [24].

As already mentioned, efficient quantum-chemical program implementations for calculations of β or the excitation energies and the R_j usually do not make explicit use of the SOS Eq. (9b) but solve equation systems that either yield the value of the linear response function at a given frequency (for calculations of optical rotation) or the excitation energies and rotatory strengths (for calculations of CD) directly. Implementations based on time-dependent DFT (TDDFT) were described, for example, in Refs. [112–120]. The reader is referred to a review by Volosov and Woody [121] for an overview of common computational methodology until about 1994, and to reviews by Polararapu [122] and Crawford [123] for overviews of more recent developments for calculating CD and optical rotation. Refs. [4,6] also contain a discussion of various theoretical approaches for calculating optical activity, with an emphasis on applications to metal complexes. Some linear-response TDDFT implementations for calculations of optical rotation allow to consider damping for the excited states [124,125] which yields both the real and the imaginary part of β from a linear response calculation at a given frequency/wavelength. Im$[\beta]$ can then directly be converted to the CD intensity. Benchmark results for organic molecules have recently confirmed that the results agree with direct computations of rotatory strengths and subsequent broadening [27]. It should be noted that the way in which an empirical damping constant has been included in these computations relates to a Lorentzian shape of the CD bands whereas, usually, in simulations of CD spectra a Gaussian broadening is applied.

Most of the older theoretical literature on CD spectra of metal complexes has been concerned with semi-empirical approaches [126–129]. Often, this has allowed a qualitative understanding of the CD of selected excitations in terms of small deviations from non chiral parent symmetries and the associated mixing of orbitals of different parent symmetries upon the chiral distortion of a complex. Unfortunately, due to the small number of excitations that are treated by such approaches and their inherent approximations, a reliable estimate of the optical rotation by employing the SOS equation cannot be obtained. It is fair to state that direct first-principles computations of CD spectra for metal complexes over the whole UV–vis accessible frequency range as well as their optical rotation have only become feasible because of the development of the relevant TDDFT techniques. The reason is, as so often, the size of a typical low-symmetry chiral metal complex which makes wave-function based correlated ab initio computations of CD spectra and optical rotation a computationally very demanding task. Hartree–Fock theory, although computationally affordable, does not yield reliable CD spectra for metal complexes. It often affords unacceptably large errors for the excitation energies. At present computer speeds, TDDFT offers an attractive balance between accuracy and efficiency. The first TDDFT computations of metal complex CD spectra started to appear in the literature in 2003 [130,131]. A preliminary calculated DFT-based CD spectrum of $[\text{Ru(bipy)}_3]^{2+}$ was presented in Fig. 7 of Ref. [129] in 1998 but no details of the method were given. To our knowledge the spectrum was not published elsewhere. In Ref. [131], Diedrich and Grimme compared TDDFT CD spectra to those obtained by a coupled-cluster (CC2) and two multireference methods (MRMP2 and DFT/MRCI). The benchmark set included a tricarbonyl-pentadienal-iron complex. However, for the transition metal complex, CC2 was not applicable and perturbative methods were found to be somewhat problematic. Acceptable agreement of the low-energy part of the CD spectrum with experiment was obtained with the B3LYP hybrid functional. TDDFT was previously found to reproduce the excitation spectra of a number of chiral Ru complexes quite well [132], but no CD computations were carried out. For a recent overview of TDDFT applied to calculate excitation energies of transition metal systems see Ref. [1]. There, Rosa et al. concluded that no hybrid nor non-hybrid functional performs consistently well for all metals, which is in line with similar conclusions for computations of NMR parameters of metal complexes [2,7,133]. We note in passing that TDDFT computations of the CD of open-shell metal complexes have been performed as well, for instance on $[\text{Co}^{\text{II}}\text{(bipy)}_3]^{2+}$ [134] or spin-triplet ground state bis(biuretato) Co^{III} complexes [135]. We will focus on the CD of singlet excitations in closed-shell metal complexes here.

4.2. *Tris-bidentate Co^{III} and Rh^{III} complexes*

In the context of optical activity, the complex $[\text{Co(en)}_3]^{3+}$ (en = ethylenediamine) has served as a typical representative for the class of tris-bidentate complexes with saturated ligands. Therefore, the optical activity of this complex has been particularly well studied. The d-to-d transitions of $[\text{Co(en)}_3]^{3+}$ and derivatives thereof have been studied extensively with crystal field and ligand field theory-based models [136–139]. We refer to reviews about transition metal CD in Refs. [127,128] for details. The ligand field theory for d-to-d transitions has also been extended to f-to-f transitions [140,141].

TDDFT computations of the CD spectra of seven tris-bidentate Co^{III} complexes (including $[\text{Co(en)}_3]^{3+}$) as well as Λ-$[\text{Rh(en)}_3]^{3+}$ were reported by Autschbach et al. in Ref. [53]. Two representative simulated spectra from Ref. [130] are shown in Fig. 12 in direct comparison with experiment. For the Λ-$[\text{Co(en)}_3]^{3+}$spectrum, the d-to-d excitation energies were found to be strongly overestimated and the ligand-to-metal charge-transfer (LMCT) excitations were underestimated in energy. In order to allow for an easier comparison with experiment in the graphics, the d-to-d transitions (CD bands α, β, γ) were red-

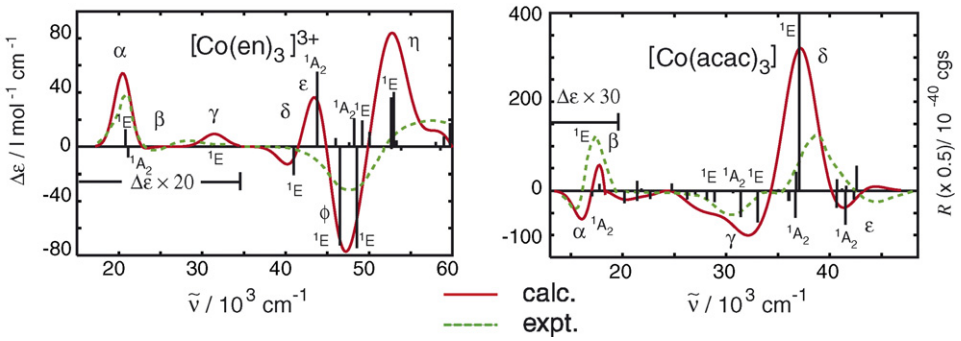

Fig. 12. CD spectra of Λ-$[Co(en)_3]^{3+}$ (ob_3-conformer) and Λ-$[Co(acac)_3]$, from Ref. [130]. Simulated CD spectra using an empirical Gaussian broadening with Gaussian line width parameter σ proportional to $\sqrt{\tilde{\nu}}$ [130]. Calculated excitation energies and rotatory strengths indicated as line spectrum. COSMO solvation model (water). For easier comparison with experiment some of the excitation energies were shifted [130], see text for details.

shifted by 6.0 $\times 10^3 cm^{-1}$ or 0.74 eV. The whole calculated spectrum for Λ-$[Co(acac)_3]$ was red-shifted by 4.0 $\times 10^3 cm^{-1}$ (0.50 eV). The errors in the calculated excitation energies can to a large extent be attributed to deficiencies in the local exchange-correlation (XC) kernel used for the TDDFT computations [130]. Further, deficiencies in the XC potential cause an overestimation of the covalent metal-d-ligand interaction which causes too large HOMO–LUMO gaps. In turn, the HOMO–LUMO gap serves as a zero-order estimate of the lowest excitation energy in TDDFT [28]. Overall, however, the agreement with experiment was deemed satisfactory.

In fact, the agreement for the CD-spectrum of Λ-$[Co(acac)_3]$ with experiment is similar as reported by Furche et al. in a pioneering TDDFT study of CD spectra of helicenes [114] (a 0.45 eV blue-shift of the calculated spectra was applied in that work). Since electronic spectra are sensitive indicators of approximations in the computations, the agreement with experiment for Λ-$[Co(acac)_3]$ can be considered as very good. For the other complexes considered for the computational study reported in Ref. [130] the agreement with experiment was not quite as good as for Λ-$[Co(acac)_3]$ but more similar to the case of Λ-$[Co(en)_3]^{3+}$. Overall, main features of the experimental CD spectra were reproduced in the computations sufficiently well in order to allow for a computational assignment of the various CD bands. The main source of errors was found to be the excitation energies, not so much the CD signs and intensities, which generally led to an acceptable shape of the simulated spectrum.

Nor too surprisingly, one of the major influences for the highly charged complexes was found to be from solvation effects. The CD spectra were measured in aqueous solution, and consequently the COSMO continuum solvation model was adopted in the computations. Fig. 13 illustrates the main findings of Autschbach et al. [130] regarding solvation effects: for triply charged complexes such as Λ-$[Co(tn)_3]^{3+}$ the inclusion of solvent effects appears to be vital since they can lead to a (blue) shift of the LMCT bands by several thousand cm^{-1}. For the lesser charged species, solvent effects considered at the continuum level did not affect the CD spectra as strongly. This becomes most obvious for the CD spectrum of the neutral Λ-$[Co(acac)_3]$ complex shown in Fig. 13. Jensen et al. have recently applied the discrete reaction field (DRF) to model solvent effects on the CD spectrum of $[Co(en)_3]^{3+}$ [142] based on molecular-dynamics simulations. The solvent effects were found to be very similar to the ones obtained from the COSMO continuum model in static computations. A certain degree of solvent broadening of the LMCT bands was obtained in the DRF computations due to the underlying molecular dynamics treatment.

We have already hinted at some of the similarities between NMR and optical activity computations because approximations in the computations may have a similar effect on the external magnetic-field perturbation of the molecule. 3d metals are notorious for posing difficulties in spectral property computations [1,4,7]. One might expect difficulties in particular when properties are considered that heavily involve the metal's d-orbitals. This is certainly the case for the d-to-d CD excitations consid-

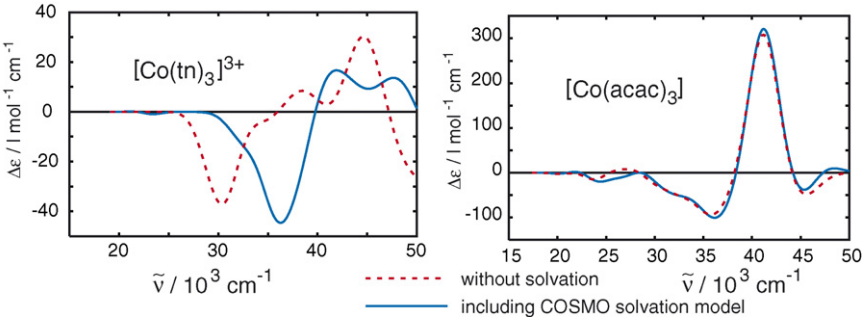

Fig. 13. CD spectra of Λ-$[Co(tn)_3]^{3+}$ and Λ-$[Co(acac)_3]$ calculated with and without a solvent model, from Ref. [130]. See also caption of Fig. 12. Excitation energies not shifted.

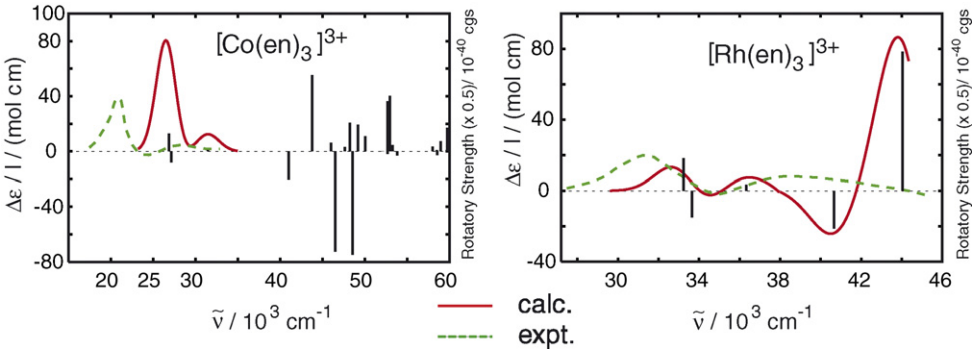

Fig. 14. CD spectra of Λ-$[Co(en)_3]^{3+}$ and Λ-$[Rh(en)_3]^{3+}$ (ob_3-conformers), from Ref. [130]. See also caption of Fig. 12. Calculated excitation energies not shifted.

ered here but also for the metal chemical shifts. For the latter, the performance of approximate DFT, in particular with non-hybrid functionals, is often better for the 4d analogs than for the 3d metals [2,7]. In Fig. 14 we compare the d-to-d range of the CD spectrum with experiment for Λ-$[Co(en)_3]^{3+}$ and Λ-$[Rh(en)_3]^{3+}$ without shifting the calculated excitation energies. It can be seen that the errors in the d-to-d excitation energies are indeed significantly smaller for the Rh complex.

In two publications, Jorge, et al. have considered the structural and electronic origin of the CD in the d-to-d and in the LMCT region. A detailed analysis of orbital contributions to the transition dipole moments made it further possible to relate the first-principles quantum-chemical results to model calculations performed over the past few decades. The first study, Ref. [143], focussed on the d-to-d optical activity in a number of Co^{III} and Rh^{III}complexes. Formally, these transitions derive from the parity-forbidden crystal-field transitions between the metal's d-levels in an octahedral environment. The question arises whether the d-to-d CD is caused by a small geometry distortion of the nitrogen ligands away from perfect octahedral symmetry or by a weak electronic coupling of the ligand's backbone orbitals, or by a combination of these and other factors. The geometric distortion can be split up into a axial and an angular component with respect to the three-fold symmetry axis of the complex, see Fig. 15 for an illustration. Jorge et al. found that the splitting and the energetic ordering of the lowest-energy (one A_2, one E) transitions, formally d-to-d HOMO–LUMO transitions, is determined by the sign and magnitude of the axial distortion (lowering the symmetry from O_h to D_{3d} and splitting the degeneracy of the HOMOs). The sign and magnitude of the angular distortion, further lowering the symmetry to D_3, determines the

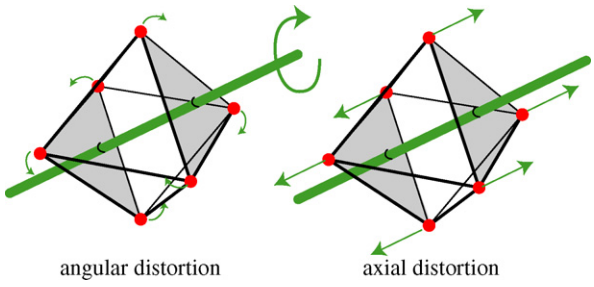

Fig. 15. Angular and axial distortions of an octahedral ligand environment to yield a D_3-symmetric chiral environment.

sign and magnitude of the rotatory strengths $R(A_2)$ and $R(E)$ for these transitions. The angular distortion mixes even (if classified by O_h-symmetry) metal orbitals with odd combinations of orbitals of the directly coordinating ligand atoms which has to vanish for an angular distortion of zero degrees. As an example for the relevance of older model theories, the contributions from combinations of even with odd metal orbitals (such as *n*d with $(n+1)$p) in the TDDFT computations provided less than 10% of the optical activity whereas this would be the only possible contribution based on crystal field theory. The second study by Jorge, et al. [144] extended the orbital-mixing model of Ref. [143] to include LMCT excitations. The extension of the model predicted that the signs of pairs of d-to-d and LMCT transitions of same symmetry are coupled and alternating, and that therefore $R(A_2)$ and $R(E)$ change sign in going from the d-to-d to the CT region, in agreement with experimental data. Further, the authors investigated the influence of conformational changes on the CD of various Co^{III} and Rh^{III} complexes with aliphatic bidentate amine ligands, i.e. the effects from the orientation of the chelate rings with respect to the threefold symmetry axis. The two possible configurations are termed ob and lel depending on whether the C–C bonds of the amine backbone are oblique or more parallel to the threefold axis. Another naming convention derives from the rotational sense δ or λ of the helical configuration of the ligand chelate ring. For instance lel_3-Λ-$[Co(en)_3]^{3+}$ is Λ($\delta\delta\delta$)-$[Co(en)_3]^{3+}$ which is the stereoisomer of lel_3-Δ-$[Co(en)_3]^{3+}$ which is Δ($\lambda\lambda\lambda$)-$[Co(en)_3]^{3+}$. However, Λ($\lambda\lambda\lambda$)-$[Co(en)_3]^{3+}$, which is ob_3-Λ-$[Co(en)_3]^{3+}$, is a diastereomer of Λ($\delta\delta\delta$)-$[Co(en)_3]^{3+}$ and may have a different CD spectrum and a different energy. In the case of $[Co(en)_3]^{3+}$ the differences in the CD are not very pronounced [130]. However, the systems studied by Jorge et al. in Ref. [144] not only involved the en (ethylenediamine) ligand but also S- and R-pn (pn = 1,2-propyl-diamine) which has a strong preference for adopting a conformation where the methyl group is equatorial to the chelate ring. By comparing a large set of experimental with computed data it was shown that the TDDFT computations correctly reproduced changes in the CD spectra due to changes in the chelate ring conformations, and that signs and intensity of the CD transitions as a function of ob versus lel conformation are a direct consequence of the sign and size of the chelate bite angle which is dictated by the preferred configuration of the rings. The configurations of the chelate rings thereby dictates the geometry of

the six nitrogens around the metal center. In turn, this geometry is mainly responsible for the sign, energetic ordering, and CD intensity of the d-to-d and LMCD transitions.

4.3. CD of metal complexes with unsaturated ligands

In the case of unsaturated ligands such as phenanthroline (phen) or bipyridyl (bipy), chiral complexes may exhibit strong exciton CD of the ligand's π-to-π* transitions, usually from coupling of excitations from two or more unsaturated ligands at the same metal center. Telfer et al. have recently reported a case of internuclear exciton CD [145]. Early theoretical studies of the CD of complexes of Fe, Ru, and Os with the ligands $phen_3$ and $bipy_3$) were, for example, performed by Mason et al. [146,147] and by Kràl et al. [148,149].

TDDFT computations of the CD spectra of the set of $[\{Fe,Ru,Os\}(phen)_3]^{2+}$ complexes were recently performed by Le Guennic et al. [51]. The authors also investigated the $bipy_3$ series (unpublished) during the course of the same study and found that the CD spectra were in similar agreement with experiment as those for the $phen_3$ systems. As an example, the CD spectrum of Λ-$[Os(phen)_3]^{2+}$ is shown in Fig. 16 along with the optimized structure of the complex. It can be seen that the agreement with experiment is even better than for the Λ-$[Co(acac)_3]$ system discussed previously. The TDDFT-based assignment of the spectrum is in agreement with the analysis of the experimental spectrum of this and similar complexes by Mason et al. [146]: the low energy part of the spectrum up to about $25 \times 10^3 cm^{-1}$ is governed by metal-to-ligand charge-transfer (MLCT) excitations (Os to ligand π*; the less intense d-to-d transitions are also in this energy range) whereas the most intense pair of CD bands between 35 and $40 \times 10^3 cm^{-1}$ is of course due to the exciton CD of the ligand π-to-π* transitions. There are also LMCT transitions occurring in this energy range. Relativistic effects on the CD spectrum, expected to be noticeable for Os, mainly cause a small red-shift on the order of $(1–2) \times 10^3 cm^{-1}$ of the CD bands α, β, and γ due to a relativistic destabilization of the metal's valence d-orbitals. Pronounced relativistic effects on higher lying states involving the metal d-orbitals hardly influence the appearance of the CD spectrum because of the dominance of the ligand π-to-π* CD bands.

Mason and co-workers who recorded the experimental spectrum [146] of the Os complex in 1969 speculated about the amount of the metal's participation in the π-to-π* exciton CD, in particular from delocalization of the π system through the metal center, as well as about the amount of ligand interaction. Trivially, of course, the metal keeps the complex together. Computation performed on Λ-$[Os(phen)_3]^{2+}$ by Le Guennic et al. [51] showed that this is indeed the metal's main function. As predicted by a coupling of the 3 long-axis polarized transition dipole moments in a Λ D_3-symmetric configuration of the complex, the most intense A_2 transition exhibits a negative Cotton effect, the E transition a positive one in the computations [51] (CD bands ε and ϕ in Fig. 16). The dissymmetry between the band intensities indicates a significant amount of interaction between the ligands. From an analysis of the orbital contributions in the TDDFT results for Λ-$[Os(phen)_3]^{2+}$ and from additional model calculations on the ligand system with and without the metal, the metal orbitals were found to contribute less than 10% to the ligand exciton CD. These 10% include possible contributions from electron delocalization through the metal center.

The spectrum for Λ-$[Ru(phen)_3]^{2+}$ was reproduced similarly well in the computations of Le Guennic et al. [51] when compared to experiment. It is also very similar to the nonrelativistic CD spectrum calculated for the Os complex which is not surprising given that the relativistic effects on the Ru valence orbital energies, roughly dependent on the nuclear charge $\sim Z^2$, are at least a factor of 3 smaller than for Os (not counting the amplifying effects from the 4f shell in Os [150]). Solvent effects did not have a strong influence on the CD spectra of any of the three complexes, which is in agreement with calculations for +2-charged Co^{III} systems [130].

The case of Λ-$[Fe(phen)_3]^{2+}$ is somewhat different from its Ru and Os analogs. Fig. 17 shows the CD spectra of this complex calculated at various levels of hybrid and non-hybrid DFT and TDDFT, in comparison with experiment. Adopting the same

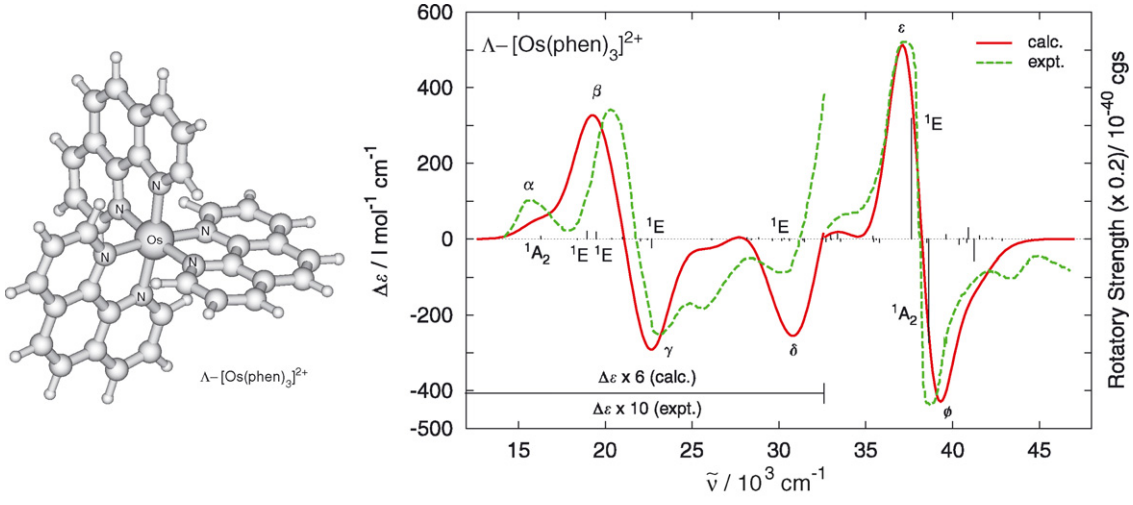

Fig. 16. Optimized structure and CD spectrum of Λ-$[Os(phen)_3]^{2+}$, from Ref. [51]. Constant Gaussian broadening of $\sigma = 0.13$ eV. Calculated excitations blue shifted by 0.2 eV.

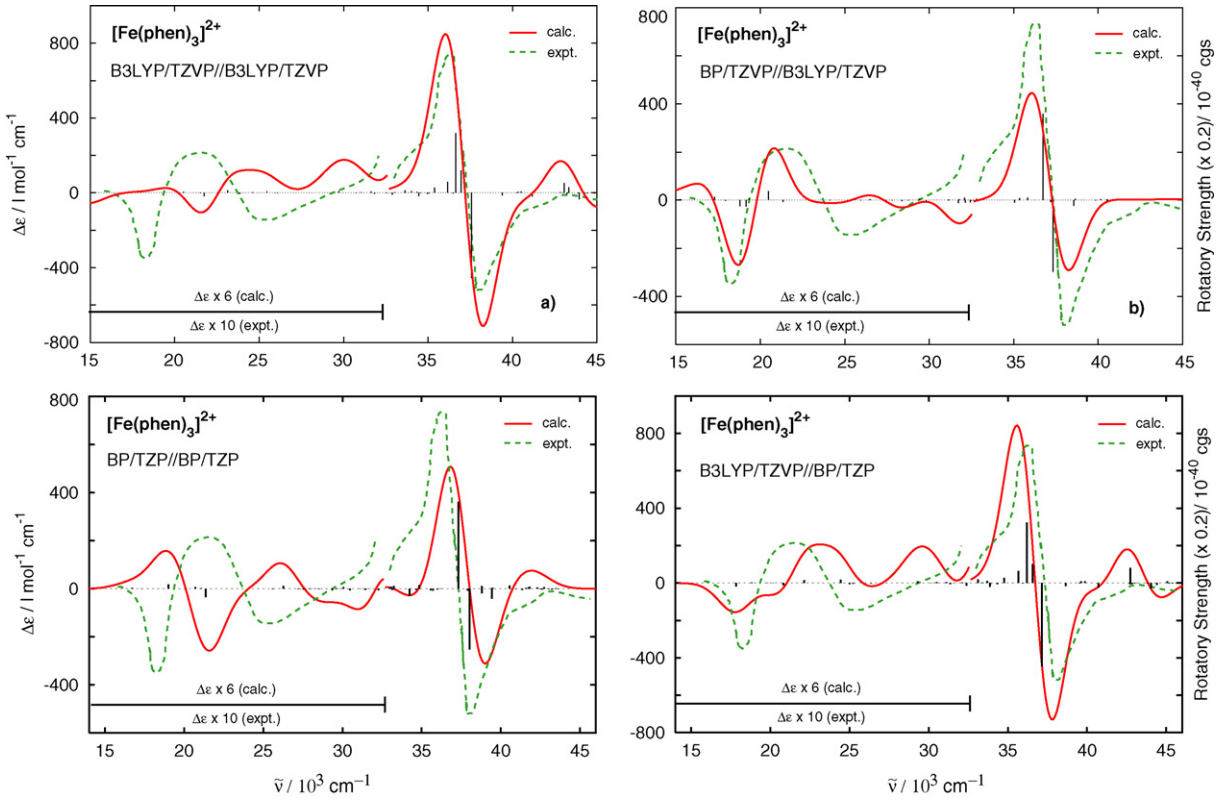

Fig. 17. CD spectra of Λ-$[Fe(phen)_3]^{2+}$ calculated at various levels of theory from Ref. [51]. TZVP Gaussian-type basis: computations with the Turbomole code. TZP Slater-type basis: computations with the ADF code. BP = non-hybrid Becke–Perdew functional, B3LYP = 3-parameter hybrid functional. The notation means: theory level used for the CD computation//theory level used for the geometry optimization. Constant Gaussian broadening with $\sigma = 0.13$ eV. BP/TZVP//PB/TZP very similar to BP/TZP//PB/TZP and therefore not shown.

strategy as used for Λ-$[Os(phen)_3]^{2+}$ and Λ-$[Ru(phen)_3]^{2+}$, i.e. using the same non-hybrid functional both for the optimization and for the TDDFT calculation of the CD, yields the spectrum at the bottom left (BP/TZP//BP/TZP). The ligand π-to-π* CD is as well reproduced as for the other two complexes, but the CD in the low-energy region has the wrong sign. Since these excitations involve metal d-orbitals this hints at similar deficiencies of the XC potential and kernel that were previously noted for Co^{III}. Indeed, by using the B3LYP hybrid functional for the CD calculation along with the non-hybrid geometry the spectrum at the bottom right is obtained, which has the correct sign also in the low-energy regime. The agreement with experiment is not great but at least the correct sign pattern is obtained. Unfortunately, when using the hybrid functional both for the optimization and for the CD computation, the agreement with experiment deteriorates (top left), whereas using the non-hybrid functional for the CD computation based on the B3LYP optimized geometry yields a very acceptable simulated spectrum (top right). Using a self-interaction free XC potential did not completely alleviate the problems, presumably because a corresponding XC kernel was not available for the computations. Future research along these lines will have to determine the exact cause of the problems associated with the low-energy part of the Λ-$[Fe(phen)_3]^{2+}$ CD spectrum. As a note aside, the CD spectra of all three complexes calculated at the non-hybrid DFT level have the same sign pattern and shape. Experimentally, the Ru and Os spectra are very similar, and match with the calculations whereas the CD spectrum of Λ-$[Fe(phen)_3]^{2+}$ has a different sign pattern in the low-energy part of the spectrum. It appears that there is a subtle balance between structural changes and a functional-dependence of the sign and energetic ordering of CD transitions for Λ-$[Fe(phen)_3]^{2+}$ that makes the experimental spectrum difficult to reproduce by computations.

4.4. Optical rotatory dispersion

Few attempts have yet been made to compute the optical rotation and the optical rotatory dispersion (ORD) for metal complexes from first-principles theory. Computations are presently under way in the author's laboratory. First results have recently been reported for the ORD of Δ-$[Co(en)_3]^{3+}$ in the visible wavelength range [125]. One complication has been the fact that the ORD of $[Co(en)_3]^{3+}$ in the visible range exhibits anomalous dispersion due to the d-to-d transitions. Most TDDFT implementations for optical rotation do not yet allow for an inclusion of damping but some programs now allow to specify a damping constant (e.g. the Dalton code [124], the ADF code [125], and NWChem (author's implementation, unpublished)). As a consequence, which is qualitatively illustrated in Fig. 18, the optical rotation calculated without damping diverges at the transition whereas it should rather follow a characteristic peak/trough pattern and pass through zero near the excitation wavelength.

In Fig. 19 we compare the computed CD and ORD for Δ-$[Co(en)_3]^{3+}$ with experimental data. In the optical rotation

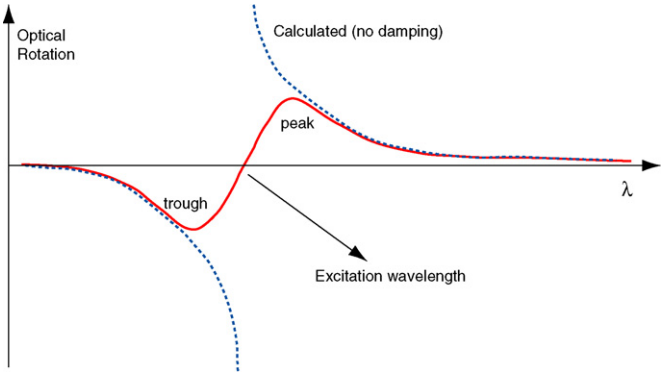

Fig. 18. Qualitative behavior of the anomalous optical rotatory dispersion(ORD) in the vicinity of an electronic transition. Here: positive Cotton effect. Without damping the calculated ORD diverges in the vicinity of the excitation as can be seen from Eq. (9b).

computations damping was applied. For reasons of theoretical consistency [27] a Lorentzian broadening was applied to the CD spectra instead of the typically used Gaussian broadening. Apart from the already discussed overestimation of the d-to-d excitation energies for $[Co(en)_3]^{3+}$ with the applied non-hybrid functional, it can be seen that the qualitative features of the ORD and its magnitude near the d-to-d transitions are in agreement with experiment when using a damping constant of same magnitude as the experimental CD line width.

Although the anomalous dispersion of the optical rotation near an electronic transition is strongly dominated by the sign and intensity of its circular dichroism, other excitations also influence the ORD. This is obvious from the SOS Eq. (9b) for β, or from the fact that by virtue of the KK transformations (12) the CD at every wavelength influences the ORD at a given wavelength. Following a recommendation by Polavarapu [151,152] the author has recently developed a program tool to perform KK transformations numerically [27]. Often, CD spectra for metal complexes over a wide frequency range are available in the literature but corresponding ORD data are not available or only over a small frequency range. In order to benchmark the performance of first-principles computations of ORD in metal complexes, it may be of benefit to compare directly with experimental data. Fig. 20 shows the experimental ORD of two metal complexes, in comparison with the KK transformation of the experimental CD. The transformations obviously had to be truncated at the upper energy limit for the experimental CD which, however, is significantly higher than the energy range over which the ORD has been measured directly. It can be seen that the ORD and the KK-transformation of the experimental CD are in qualitative agreement, although the influence of high-energy excitations is clearly not negligible. Systematic deviations between ORD and

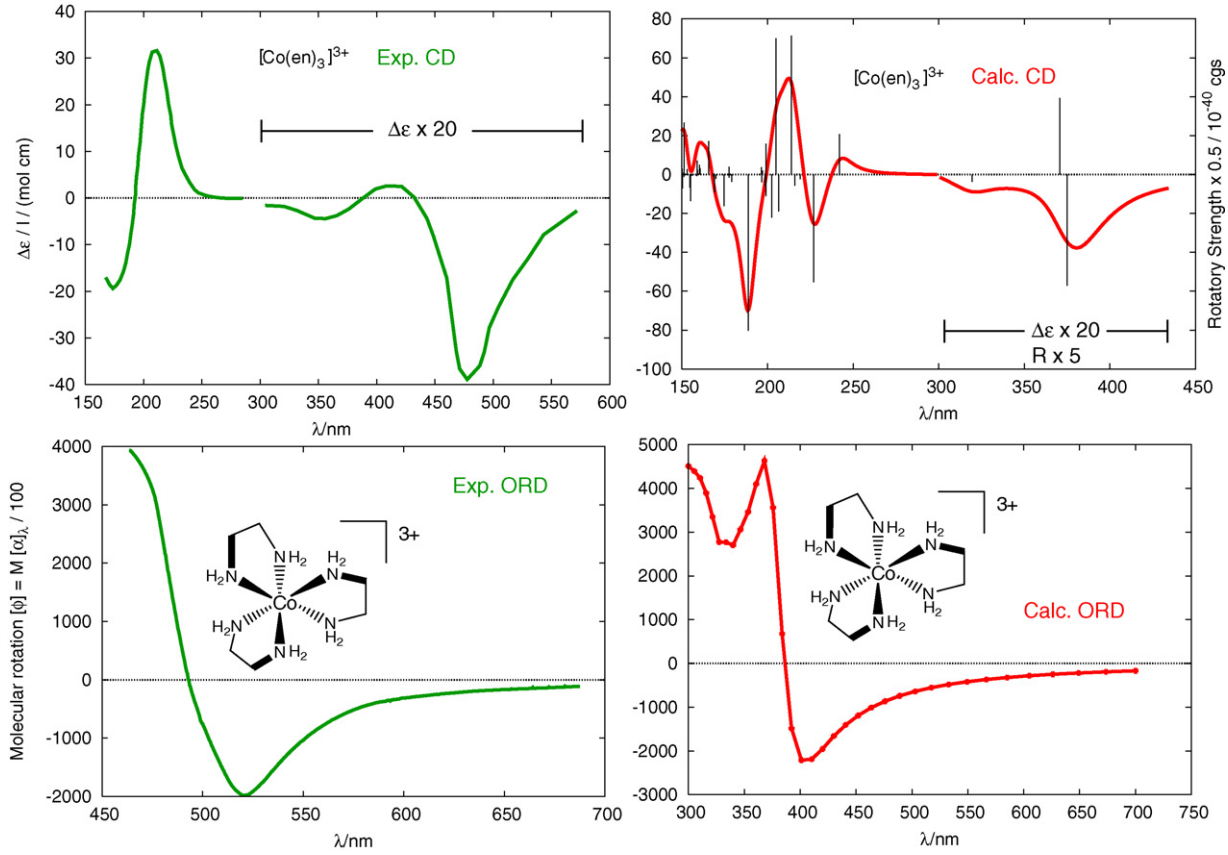

Fig. 19. Experimental and calculated CD and ORD of Δ-$[Co(en)_3]^{3+}$ in the UV–vis range, from Ref. [125]. ORD was calculated with non-hybrid DFT using a damping constant Γ for the excited states of 0.2 eV. Lorentzian broadening was applied to the computed CD using the same value of Γ for the line width at half peak height. Calculated excitation energies not shifted.

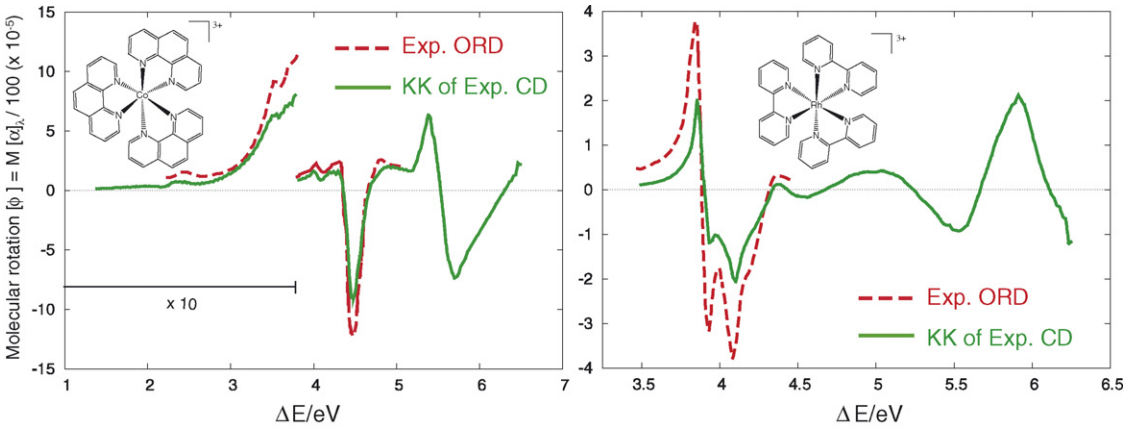

Fig. 20. Experimental ORD and numerical Kramer–Kronig (KK) transformation of experimental CD spectrum for two metal-(phen)$_3$ complexes. Experimental data from Refs. [153,154]

KK-transformed CD, or vice versa, might also provide useful information about high lying excited states not directly accessible spectroscopically (see Polavarapu, Ref. [152]). In other cases where experimental ORD is not available, KK-transformations of experimental CD spectra may be useful to allow an assessment of the performance of ORD computations.

5. Summary

DFT-based theoretical methods for energy-derivative properties have matured to a point where computations on metal complexes can be performed on a routine basis. Although such DFT methods are not without shortcomings, in many cases useful insight into the mechanisms responsible for the sign, magnitude, and trends of experimental data has been gained from first-principles computations. In this paper, theoretical work related to magnetic-field perturbations of metal complexes has been discussed. Among other important optical and spectroscopic parameters, the basic observables of NMR as well as of electronic optical activity can be computed from linear response functions that involve a static or dynamic magnetic field. It has been demonstrated by a range of applications of DFT and TDDFT-based theoretical methods that their overall performance for metal complexes is quite good. The methods are general in the sense that they are not specifically geared towards metal complexes but they may as well be applied to organic molecules, for example. Relativistic methods allow computations on molecules that contain elements from all parts of the periodic table. It was shown that the inclusion of solvent effects can be vital for reproducing experimental results that were obtained in solution. NMR parameters of metal complexes appear to be particularly sensitive to such solvent effects.

Acknowledgments

The author is grateful to his collaborators as well as former and present co-workers Drs. Boris Le Guennic, Mykhaylo Krykunov, and Mariusz Sterzel, and graduate students Shaohui Zheng, Mark Rudolph, Matthew Kundrat, and Brendan C. Mort, for their contributions and collaboration on the research projects discussed in this article. Special thanks to A. Bagno and D. Gusev for providing electronic versions of some of the figures used in their publications. Further, the author gratefully acknowledges support from the Center for Computational research at SUNY Buffalo and financial support from the Career program of the National Science Foundation and from the donors of the ACS Petroleum Research Fund. Some of the computations were performed as part of the Molecular Sciences Computing Facility (MSCF) Grand Challenge project entitled “Reliable Electronic Structure Calculations for Heavy Element Chemistry: Molecules Containing Actinides, Lanthanides and Transition Metals” at the Environmental Molecular Science Laboratory located at the Pacific Northwest National Laboratory.

References

[1] A. Rosa, G. Ricciardi, O. Gritsenko, E.J. Baerends, Excitation energies of metal complexes with time-dependent density functional theory, in: N. Kaltsoyannis, J.E. McGrady (Eds.), Principles and Applications of Density Functional Theory in Inorganic Chemistry I, vol. 112 of Structure and Bonding, Springer, Heidelberg, 2004, p. 49.
[2] J. Autschbach, The calculation of NMR parameters in transition metal complexes, in: N. Kaltsoyannis, J.E. McGrady (Eds.), Principles and Applications of Density Functional Theory in Inorganic Chemistry I, vol. 112 of Structure and Bonding, Springer, Heidelberg, 2004, p. 1.
[3] J. Autschbach, T. Ziegler, Relativistic calculation of spin–spin coupling constants, in: M. Kaupp, M. Bühl, V.G. Malkin (Eds.), Calculation of NMR and EPR Parameters. Theory and Applications, Wiley-VCH, Weinheim, 2004.
[4] J. Autschbach, T. Ziegler, Coord. Chem. Rev. 238/239 (2003) 83.
[5] J. Autschbach, Calculation of heavy-nucleus chemical shifts: relativistic all-electron methods, in: M. Kaupp, M. Bühl, V.G. Malkin (Eds.), Calculation of NMR and EPR Parameters. Theory and Applications, Wiley-VCH, Weinheim, 2004.
[6] T. Ziegler, J. Autschbach, Chem. Rev. (2005) 2695.
[7] M. Bühl, NMR of transition metal compounds, in: M. Kaupp, M. Bühl, V.G. Malkin (Eds.), Calculation of NMR and EPR Parameters. Theory and Applications, Wiley-VCH, Weinheim, 2004, p. 421.
[8] M. Kaupp, V.G. Malkin, O.L. Malkina, NMR of transition metal compounds, in: P. von Ragué Schleyer (Ed.), Encyclopedia of Computational Chemistry, John Wiley & Sons, Chichester, 1998, p. 1857.
[9] A. Bagno, G. Saielli, Computational NMR spectroscopy: reversing the information flow, Theor. Chem. Acc. 117 (2007) 603.

[10] M. Kaupp, M. Bühl, V.G. Malkin (Eds.), Calculation of NMR and EPR Parameters. Theory and Applications, Wiley-VCH, Weinheim, 2004.
[11] F. Neese, Applications to EPR in bioinorganic chemistry, in: M. Kaupp, M. Bühl, V.G. Malkin (Eds.), Calculation of NMR and EPR Parameters. Theory and Applications, Wiley-VCH, Weinheim, 2004, p. 581.
[12] T. Ziegler, J. Chem. Soc. Dalton Trans. (2002) 642.
[13] W. Koch, M.C. Holthausen, A Chemist's Guide to Density Functional Theory, Wiley-VCH, Weinheim, 2001.
[14] O. Christiansen, P. Jørgensen, C. Hättig, Int. J. Quantum Chem. 68 (1998) 1.
[15] S.T. Epstein, The Variation Method in Quantum Chemistry, Academic Press, New York, 1974.
[16] J. Gauss, Molecular properties, in: J. Grotendorst (Ed.), Modern Methods and Algorithms of Quantum Chemistry, vol. 3 of NIC, John von Neumann Institute for Computing, Jülich, 2000, p. 541.
[17] H.F. King, A. Komornicki, J. Chem. Phys. 84 (1986) 5645.
[18] J. Oddershede, Propagator methods, in: K.P. Lawley (Ed.), Ab initio Methods in Quantum Chemistry, vol. II, John Wiley & Sons, London, 1987, p. 201.
[19] T. Helgaker, K. Ruud, K.L. Bak, P. Jørgensen, J. Olsen, Faraday Discuss 99 (1994) 165.
[20] J. Gauss, H.J. Werner, Phys. Chem. Chem. Phys. 2 (2000) 2083.
[21] M. Krykunov, J. Autschbach, J. Chem. Phys. 123 (2005) 114103.
[22] W. Kauzmann, Quantum Chemistry, Academic Press, New York, 1957.
[23] F.W. Byron, R.W. Fuller, The Mathematics of Classical and Quantum Physics, Addison-Wesley, Reading, Mass, 1969.
[24] A. Moscowitz, Adv. Chem. Phys. 4 (1962) 67.
[25] J.A. Schellman, Chem. Rev. 75 (1975) 748.
[26] L.D. Barron, Molecular Light Scattering and Optical Activity, 2nd ed., Cambridge University Press, 2004.
[27] M. Krykunov, M.D. Kundrat, J. Autschbach, J. Chem. Phys. 125 (2006) 194110.
[28] M.E. Casida, Time-dependent density functional response theory for molecules, in: D.P. Chong (Ed.), Recent Advances in Density Functional Methods, vol. 1, World Scientific, Singapore, 1995, p. 155.
[29] S.P.A. Sauer, M.J. Packer, The ab initio calculation of molecular properties other than the potential energy surface, in: P.R. Bunker, P. Jensen (Eds.), Computational Molecular Spectroscopy, John Wiley & Sons, London, 2000, p. 221.
[30] B.E. Mann, Rhodium-103, in: P.S. Pregosin (Ed.), Transition Metal Nuclear Magnetic Resonance, Elsevier, Amsterdam, 1991, p. 177.
[31] M. Bühl, S. Gaemers, C.J. Elsevier, Chem. Eur. J. 6 (2000) 3272.
[32] J. Autschbach, T. Ziegler, Relativistic computation of NMR shieldings and spin–spin coupling constants, in: D.M. Grant, R.K. Harris (Eds.), Encyclopedia of Nuclear Magnetic Resonance, vol. 9, John Wiley & Sons, Chichester, 2002, p. 306.
[33] P. Pyykkö, Chem. Rev. 88 (1988) 563.
[34] W.H.E. Schwarz, Fundamentals of Relativistic Effects in Chemistry, in: Z.B. Masic (Ed.), The Concept of the Chemical Bond, vol. 2, Springer, Berlin, 1990, p. 559.
[35] B.A. Hess, Relativistic theory and applications, in: P. von Ragué Schleyer (Ed.), Encyclopedia of Computational Chemistry, John Wiley & Sons, Chichester, 1998, p. 2499.
[36] P. Pyykkö, J. Organomet. Chem. 232 (1982) 21.
[37] D.L. Bryce, R.E. Wasylishen, J. Autschbach, T. Ziegler, J. Am. Chem. Soc. 124 (2002) 4894.
[38] J. Autschbach, T. Ziegler, J. Chem. Phys. 113 (3) (2000) 9410.
[39] K.E. Berg, J. Glaser, M.C. Read, I. Tóth, J. Am. Chem. Soc. 117 (1995) 7550.
[40] M. Maliarik, K. Berg, J. Glaser, M. Sandström, I. Tóth, Inorg. Chem. 37 (1998) 2910.
[41] W. Chen, F. Liu, K. Matsumoto, J. Autschbach, B. Le Guennic, T. Ziegler, M. Maliarik, J. Glaser, Inorg. Chem. 45 (2006) 4526.
[42] B. Le Guennic, K. Matsumoto, J. Autschbach, Magn. Res. Chem. 42 (2004) S99.
[43] J. Autschbach, T. Ziegler, J. Am. Chem. Soc. 123 (2001) 5320.
[44] J. Autschbach, B. Le Guennic, J. Am. Chem. Soc. 125 (2003) 13585.
[45] A. Klamt, G. Schüürmann, J. Chem. Soc. Perkin Trans. 2 (1993) 799.
[46] C.C. Pye, T. Ziegler, Theor. Chem. Acc. 101 (1999) 396.
[47] P.R.T. Schipper, O.V. Gritsenko, S.J.A. van Gisbergen, E.J. Baerends, J. Chem. Phys. 112 (3) (2000) 1344.
[48] J. Poater, E. van Lenthe, E.J. Baerends, J. Chem. Phys. 118 (19) (2003) 8584.
[49] J. Autschbach, T. Ziegler, J. Am. Chem. Soc. 123 (2001) 3341.
[50] J. Autschbach, C.D. Igna, T. Ziegler, J. Am. Chem. Soc. 125 (16) (2003) 4937.
[51] B. Le Guennic, W. Hieringer, A. Görling, J. Autschbach, J. Phys. Chem. A 109 (2005) 4836.
[52] J. Autschbach, B. Le Guennic, J. Chem. Educ. 84 (2007) 156.
[53] J. Autschbach, C.D. Igna, T. Ziegler, J. Am. Chem. Soc. 125 (2003) 1028.
[54] G.W. Proctor, F. Yu, Phys. Rev. 81 (1) (1951) 20.
[55] A. von Zelevsky, Helv. Chim. Acta 51 (1968) 803.
[56] P.S. Pregosin, Annu. Rep. NMR. Spectrosc. 17 (1986) 285.
[57] T.M. Gilbert, T. Ziegler, J. Phys. Chem. A 103 (1999) 7535.
[58] S.K. Wolff, T. Ziegler, J. Chem. Phys. 109 (3) (1998) 895.
[59] J. Autschbach, B. Le Guennic, Chem. Eur. J. 10 (2004) 2581.
[60] J. Kramer, K. Koch, Inorg. Chem. 45 (2006) 7843.
[61] K.R. Koch, M.R. Burger, J. Kramer, A.N. Westra, Dalton Trans. (2006) 3277.
[62] S.K. Wolff, T. Ziegler, E. van Lenthe, E.J. Baerends, J. Chem. Phys. 110 (16) (1999) 7689.
[63] M. Sterzel, J. Autschbach, Inorg. Chem. 45 (2006) 3316.
[64] K. Matsumoto, S. Arai, M. Ochiai, W. Chen, A. Nakata, S. Nakai, H. Kinoshita, Inorg. Chem. 44 (2005) 8552.
[65] M. Bühl, F.T. Mauschick, Phys. Chem. Chem. Phys. 4 (2002) 5508.
[66] M. Bühl, F.T. Mauschick, F. Terstegen, B. Wrackmeyer, Angew. Chem. Int. Ed. 41 (13) (2002) 2312.
[67] M. Bühl, S. Grigoleit, H. Kabrede, F.T. Mauschick, Chem. Eur. J. 12 (2006) 477.
[68] J. Autschbach, S. Zheng, Magn. Reson. Chem. 44 (2006) 989.
[69] K.J. Ooms, R.E. Wasylishen, J. Am. Chem. Soc. 126 (2004) 10972.
[70] A. Bagno, M. Bonchio, Eur. J. Inorg. Chem. (2002) 1475.
[71] A. Bagno, M. Bonchio, Magn. Reson. Chem 42 (2004) S79.
[72] J. Autschbach, B.A. Hess, P.A. Johansson, J. Neugebauer, M. Patzschke, P. Pyykkö, M. Reiher, D. Sundholm, Phys. Chem. Chem. Phys. 6 (2004) 11.
[73] P. Pyykkö, N. Runeberg, Angew. Chem. Int. Ed. 41 (2002) 2174.
[74] X. Li, B. Kiran, J. Li, H.-J. Zhai, L.-S. Wang, Angew. Chem. Int. Ed. 41 (2002) 4786 (Angew. Chem. 114, 4980–4983).
[75] A. Rodriguez-Fortea, P. Alemany, T. Ziegler, J. Phys. Chem. A 103 (1999) 8288.
[76] B. Le Guennic, J. Neugebauer, M. Reiher, J. Autschbach, Chem. Eur. J. 11 (2005) 1677.
[77] F. Scherbaum, A. Grohmann, B. Huber, C. Krüger, H. Schmidbaur, Angew. Chem. 100 (1988) 1602.
[78] F. Scherbaum, A. Grohmann, B. Huber, C. Krüger, H. Schmidbaur, Angew. Chem., Int. Ed. 27 (1988) 1544 (Angew. Chem. 1998, 100, 1602–1604).
[79] V.G. Albano, D. Braga, S. Martinengo, J. Chem. Soc., Dalton Trans. 3 (1981) 717.
[80] V.G. Albano, M. Sanson, P. Chini, S. Martinengo, J. Chem. Soc., Dalton Trans. 6 (1973) 651.
[81] M.R. Churchill, J. Wormald, J. Chem. Soc., Dalton Trans. 22 (1974) 2410.
[82] J.S. Bradley, G.B. Ansell, M.E. Leonowicz, E.W. Hill, J. Am. Chem. Soc. 103 (1981) 4968.
[83] P.F. Jackson, B.F.G. Johnson, J. Lewis, J.N. Nicholls, M. McPartlin, W.J.H. Nelson, J. Chem. Soc., Chem. Commun. 12 (1980) 564.
[84] A. Görling, N. Rösch, D.E. Ellis, H. Schmidbaur, Inorg. Chem. 30 (1991) 3986.
[85] M. Kaupp, Chem. Commun. (1996) 1141–1142.
[86] J.D. Harris, T. Hughbanks, J. Am. Chem. Soc. 119 (1997) 9449.
[87] J. Shen, T. Hughbanks, J. Phys. Chem. A 108 (2004) 350.
[88] H. Schmidbaur, B. Brachthäuser, O. Steigelmann, Angew. Chem., Int. Ed. 30 (1991) 1488 (Angew. Chem. 1991, 103, 1552–1553).

[89] M. Kaupp, O.L. Malkina, V.G. Malkin, P. Pyykkö, Chem. Eur. J. 4 (1) (1998) 118.
[90] J. Gracia, J.M. Poblet, J. Autschbach, L.P. Kazansky, Eur. J. Inorg. Chem. (2006) 1139.
[91] J. Autschbach, E. Zurek, J. Phys. Chem. A 107 (2003) 4967.
[92] J. Gracia, J.M. Poblet, J.A. Fernández, J. Autschbach, L.P. Kazansky, Eur. J. Inorg. Chem. (2006) 1149.
[93] A. Bagno, M. Bonchio, J. Autschbach, Chem. Eur. J. 12 (2006) 8460.
[94] A. Bagno, M. Bonchio, Chem. Phys. Lett. 317 (2000) 123.
[95] D.M. Heinekey, W.J.J. Oldham, Chem. Rev. 93 (1993) 913.
[96] D. Gusev, J. Am. Chem. Soc. 126 (2004) 14249.
[97] J.S. Craw, G.B. Bacskay, N.S. Hush, J. Am. Chem. Soc. 116 (1994) 5937.
[98] G.B. Bacskay, I. Bytheway, N.S. Hush, J. Am. Chem. Soc. 118 (1996) 3753.
[99] B. Le Guennic, S. Patchkovskii, J. Autschbach, J. Chem. Theor. Comput. 1 (2005) 601.
[100] T.A. Ruden, O.B. Lutnæs, T. Helgaker, K. Ruud, J. Chem. Phys. 118 (21) (2003) 9572.
[101] J. Kowalewski, Annu. Rep. NMR Spectrosc. 12 (1982) 81.
[102] B.C. Mort, J. Autschbach, J. Am. Chem. Soc. 128 (2006) 10060.
[103] B.C. Mort, J. Autschbach, J. Phys. Chem. A 110 (2006) 11381.
[104] B.C. Mort, J. Autschbach, J. Phys. Chem. A 109 (2005) 8617.
[105] D.M. Heinekey, A.S. Hinkle, J.D. Close, J. Am. Chem. Soc. 118 (1996) 5353.
[106] V. Pons, D.M. Heinekey, J. Am. Chem. Soc. 125 (2003) 8428.
[107] R. Gelabert, M. Moreno, J.M. Lluch, A. Lledós, D.M. Heinekey, J. Am. Chem. Soc. 127 (2005) 5632.
[108] D.G. Gusev, private communication.
[109] A.D. Buckingham, Adv. Chem. Phys. 12 (1967) 107.
[110] R.D. Amos, Chem. Phys. Lett. 87 (1982) 23.
[111] E.U. Condon, Rev. Mod. Phys. 9 (1937) 432.
[112] J.R. Cheeseman, M.J. Frisch, F.J. Devlin, P.J. Stephens, J. Phys. Chem. A 104 (5) (2000) 1039.
[113] P.J. Stephens, F.J. Devlin, J.R. Cheeseman, M.J. Frisch, J. Phys. Chem. A 105 (22) (2001) 5356.
[114] F. Furche, R. Ahlrichs, C. Wachsmann, E. Weber, A. Sobanski, F. Vögtle, S. Grimme, J. Am. Chem. Soc. 122 (8) (2000) 1717.
[115] S. Grimme, Chem. Phys. Lett. 339 (2001) 380.
[116] J. Autschbach, T. Ziegler, J. Chem. Phys. 116 (3) (2002) 891.
[117] J. Autschbach, T. Ziegler, S.J.A. van Gisbergen, E.J. Baerends, J. Chem. Phys. 116 (2002) 6930.
[118] J. Autschbach, T. Ziegler, S. Patchkovskii, S.J.A. van Gisbergen, E.J. Baerends, J. Chem. Phys. 117 (2002) 581.
[119] K. Ruud, T. Helgaker, Chem. Phys. Lett. 352 (2002) 533.
[120] M. Pecul, K. Ruud, T. Helgaker, Chem. Phys. Lett. 388 (2004) 110.
[121] A. Volosov, R.W. Woody, Theoretical approach to natural electronic optical activity, in: K. Nakanishi, N. Berova, R.W. Woody (Eds.), Circular Dichroism. Principles and Applications, VCH, New York, 1994.
[122] P.L. Polavarapu, Chirality 14 (2002) 768.
[123] T.D. Crawford, Theor. Chem. Acc. 115 (4) (2006) 227.
[124] P. Norman, K. Ruud, T. Helgaker, J. Chem. Phys. 120 (11) (2004) 5027.
[125] J. Autschbach, L. Jensen, G.C. Schatz, Y.C.E. Tse, M. Krykunov, J. Phys. Chem. A 110 (2006) 2461.
[126] C.J. Ballhausen, Molecular Electronic Structures of Transition Metal Complexes, McGraw-Hill, London, 1979.
[127] R. Kuroda, Y. Saito, Circular dichroism of inorganic complexes: Interpretation and applications, in: N. Berova, K. Nakanishi, R.W. Woody (Eds.), Circular Dichroism: Principles and Applications, 2nd ed., VCH, New York, 2000.
[128] B.E., Douglas, Y., Saito, (Eds.), Stereochemistry of Optically Active Transition Metal Compounds, vol. 119 of ACS Symposium Series, Americal Chemical Society, Washington, 1980.
[129] M. Ziegler, A. von Zelewsky, Coord. Chem. Rev. 177 (1998) 257.
[130] J. Autschbach, F.E. Jorge, T. Ziegler, Inorg. Chem. 42 (9) (2003) 2867.
[131] C. Diedrich, S. Grimme, J. Phys. Chem. A 107 (14) (2003) 2524.
[132] S.I. Gorelsky, A.B.P. Lever, J. Organomet. Chem. 635 (2001) 187.
[133] M. Bühl, Magn. Reson. Chem. 44 (2006) 661.
[134] A. Vargas, M. Zerara, E. Krausz, A. Hauser, L.M. Lawson Daku, J. Chem. Theor. Comput. 2 (2006) 1342.
[135] P.W. Thulstrup, E. Larsen, Dalton Trans. 14 (2006) 1784.
[136] S.F. Mason, R.H. Seal, Mol. Phys. 31 (3) (1976) 755.
[137] P.E. Schipper, J. Am. Chem. Soc. 100 (5) (1978) 1433.
[138] R.W. Strickland, F.S. Richardson, Inorg. Chem. 12 (5) (1973) 1025.
[139] R.S. Evans, A.F. Schreiner, P.J. Hauser, Inorg. Chem. 13 (9) (1974) 2185.
[140] F.S. Richardson, T.R. Faulkner, J. Chem. Phys. 76 (4) (1982) 1595.
[141] J.D. Saxe, T.R. Faulkner, F.S. Richardson, J. Chem. Phys. 76 (4) (1982) 1607.
[142] L. Jensen, M. Swart, P. Th. van Duijnen, J. Autschbach, Int. J. Quantum Chem. 106 (2006) 2479.
[143] F.E. Jorge, J. Autschbach, T. Ziegler, Inorg. Chem. 42 (2004) 8902.
[144] F.E. Jorge, J. Autschbach, T. Ziegler, J. Am. Chem. Soc. 127 (2005) 975.
[145] S.G. Telfer, N. Tajima, R. Kuroda, J. Am. Chem. Soc. 126 (2004) 1408.
[146] A.J. McCaffery, S.F. Mason, B.J. Norman, J. Chem. Soc. A (1969) 1428.
[147] S.F. Mason, B.J. Norman, J. Chem. Soc. A (1969) 1442.
[148] M. Král, A. Moscowitz, C.J. Ballhausen, Theor. Chim. Acta 30 (1973) 339.
[149] M. Král, Theor. Chim. Acta 50 (1979) 355.
[150] J. Autschbach, S. Sikierski, P. Schwerdtfeger, M. Seth, W.H.E. Schwarz, J. Comput. Chem. 23 (2002) 804.
[151] P.L. Polavarapu, J. Phys. Chem. A 109 (2005) 7013.
[152] P.L. Polavarapu, Chirality 18 (5) (2006) 348.
[153] S.F. Mason, B.J. Peart, J. Chem. Soc. Dalton Trans. 9 (1973) 949.
[154] L.S. Dollimore, R.D. Gillard, J. Chem. Soc. Dalton Trans. 9 (1973) 933.